Prompt and nonprompt J/ production and nuclear modification in pPb collisions at sNN=8.16 TeV

Aaij, R.; Adeva, B.; Adinolfi, M.; Ajaltouni, Z.; Akar, S.; Albrecht, J.; Alessio, F.; Alexander, M.; Alfonso Albero, A.; Ali, S.; Alkhazov, G.; Alvarez Cartelle, P.; Alves, A. A.; Amato, S.; Amerio, S.; Amhis, Y.; An, L.; Anderlini, L.; Andreassi, G.; Andreotti, M.

Prompt and nonprompt J/ψ production and nuclear modification in pPb collisions at $\sqrt{s_{NN}} = 8.16$ TeV

LHCb Collaboration

ARTICLE INFO

ABSTRACT

The production of J/ψ mesons is studied in proton-lead collisions at the centre-of-mass energy per nucleon pair $\sqrt{s_{NN}} = 8.16$ TeV with the LHCb detector at the LHC. The double differential cross-sections of prompt and nonprompt J/ψ production are measured as a function of the J/ψ transverse momentum and rapidity in the nucleon–nucleon centre-of-mass frame. Forward-to-backward ratios and nuclear modification factors are determined. The results are compared with theoretical calculations based on collinear factorisation using nuclear parton distribution functions, on the colour glass condensate or on coherent energy loss models.

1. Introduction

The production of J/ψ mesons, and more generally of quarkonium states, has been considered as a sensitive probe of colour screening in a hot and dense medium since the proposal by Matsui and Satz in 1986 [1] of the suppression of the J/ψ meson production in heavy-ion collisions as a sign of deconfinement. The theoretical understanding of the bound-state dynamics of quarkonium by means of lattice QCD and effective field theories has progressed substantially in the last 30 years. In heavy-ion collisions, the emerging picture indicates strong modifications of the quarkonium bound-state characteristics [2]. Experimentally, measurements at the SPS, RHIC and LHC revealed interesting patterns [3]. In particular, an additional low transverse momentum (p_T) component of J/ψ production was observed in PbPb collisions at the LHC [4–8]. This observation had been predicted as a sign of charmonium originating from unbound charm quarks, generated either during the lifetime of the deconfined medium [9] or at the phase boundary [10].

The limited understanding of nuclear phenomena unrelated to deconfinement, commonly called cold nuclear matter (CNM) effects, restricts the ability of phenomenological models to describe the experimental data on J/ψ production in PbPb collisions. The size of CNM effects can be quantified by measurements in proton-nucleus or deuteron-nucleus collisions, which have been pursued at fixed target experiments as well as at RHIC and LHC [3]. The feature of CNM drawing the highest attention for proton-lead collisions at the LHC is the modification of the gluon flux coupling to the charm quark pair. This modification is often treated within a collinear parton distribution framework employing nuclear parton distribution functions (nPDFs) [11–15]. At low longitudinal mo-

mentum fractions x carried by the parton, calculations within the colour glass condensate (CGC) effective field theory, describing the saturation regime of QCD [16,17], are frequently employed. Several calculations have been pursued to quantify nuclear modifications of J/ψ production in the collinear framework [18–21] or in the CGC framework [22–24]. It has to be noted that the low-x gluon content of the nucleus is largely unconstrained by experimental data at perturbative scales. In addition, small-angle gluon radiation taking into account interference between initial and final state radiation, called coherent energy loss, was proposed as the dominant nuclear modification of quarkonium production in proton-lead collisions [25]. The discrimination between these phenomena is a strong motivation for the study of the production of quarkonium as a hard-scale probe of QCD at high density.

The experimental results on J/ψ production in proton-lead collisions based on the 2013 data samples at $\sqrt{s_{NN}} = 5$ TeV published by the LHC experiments ALICE, ATLAS, CMS and LHCb [26–31] can be qualitatively described by implementations of the approaches described above in the kinematic applicability range of the calculations [18–21,23–25]. No conclusion on the dominant mechanism for nuclear modification of J/ψ production could be drawn.

The measurement of an additional suppression of the excited state $\psi(2S)$ by ALICE [32,33] and LHCb [34] in proton-lead collisions at $\sqrt{s_{NN}} = 5$ TeV and by PHENIX at RHIC [35,36] in various collision systems at $\sqrt{s_{NN}} = 0.2$ TeV cannot be explained by the modification of the gluon flux or by coherent energy loss because it would affect the J/ψ and the $\psi(2S)$ states in a similar way. These measurements motivated calculations involving hadronic and partonic interactions influencing the evolution of the $c\bar{c}$ pair after the first interaction [37,38] for proton(deuteron)-nucleus collisions. Although the impact on J/ψ production is generally small

in these models, it can be significant in rapidity ranges with large particle densities.

The measurement of the nonprompt J/ψ production provides access to the production of beauty hadrons. The modification of their kinematic distributions in nucleus–nucleus collisions carries valuable information about the created matter [3]. Similarly to direct charmonium production, the production of beauty hadrons can be subject to CNM effects altering the interpretation of nucleus–nucleus collision data. Such effects can be precisely measured in proton-lead collisions.

The measurements of the production of prompt J/ψ and nonprompt J/ψ mesons, called J/ψ-from-b-hadrons in the following, presented in this letter are important ingredients for the understanding of the imprints of deconfinement in nucleus–nucleus collisions. They are based on larger integrated luminosities and on higher collision energies than the initial measurements with the 2013 proton-lead data sample by the LHCb experiment at $\sqrt{s_{NN}} = 5$ TeV [27].

2. Detector, data sample and observables

The LHCb detector [39,40] is a single-arm forward spectrometer covering the pseudorapidity range $2 < \eta < 5$, designed for the study of particles containing b or c quarks. The detector includes a high-precision tracking system consisting of a silicon-strip vertex detector surrounding the interaction region [41], a large-area silicon-strip detector located upstream of a dipole magnet with a bending power of about 4 Tm, and three stations of silicon-strip detectors and straw drift tubes [42] placed downstream of the magnet. The tracking system provides a measurement of momentum of charged particles with a relative uncertainty that varies from 0.5% at low momentum to 1.0% at 200 GeV/c. The minimum distance of a track to a primary vertex (PV), the impact parameter, is measured with a resolution of $(15 + 29/p_T)$ µm, where p_T is the transverse momentum in the LHCb frame, in GeV/c. Different types of charged hadrons are distinguished using information from two ring-imaging Cherenkov detectors [43]. Photons, electrons and hadrons are identified by a calorimeter system consisting of scintillating-pad and preshower detectors, an electromagnetic calorimeter and a hadronic calorimeter. Muons are identified by a system composed of alternating layers of iron and multiwire proportional chambers [44].

This analysis is based on data acquired during the 2016 LHC heavy-ion run, where protons and ^{208}Pb ions were colliding at a centre-of-mass energy per nucleon pair of $\sqrt{s_{NN}} = 8.16$ TeV. Since the energy per nucleon in the proton beam is larger than in the lead beam, the nucleon–nucleon centre-of-mass system has a rapidity in the laboratory frame of 0.465 (-0.465), when the proton (lead) beam travels from the vertex detector towards the muon chambers. Consequently, the LHCb detector covers two different acceptance regions:

1. $1.5 < y^* < 4.0$ when the proton beam travels from the vertex detector towards the muon chambers,
2. $-5.0 < y^* < -2.5$ when the proton beam travels from the muon chambers towards the vertex detector,

where y^* is the rapidity in the centre-of-mass frame of the colliding nucleons, with respect to the proton beam direction. In this letter, the first configuration is denoted pPb and the second one Pbp. The data samples correspond to an integrated luminosity of 13.6 ± 0.3 nb^{-1} of pPb collisions and 20.8 ± 0.5 nb^{-1} of Pbp collisions. The instantaneous luminosity for the majority of the recorded events ranges between 0.5 and 1.0×10^{29} cm^{-2}s^{-1}. This

luminosity corresponds on average to about 0.1 or fewer collisions per bunch crossing.

In this letter, we describe the measurement of the double-differential production cross-sections of J/ψ mesons as a function of p_T and y^* in the ranges $0 < p_T < 14$ GeV/c and $1.5 < y^* < 4.0$ for pPb and $-5.0 < y^* < -2.5$ for Pbp. The measurement is performed separately for prompt J/ψ mesons, *i.e.* produced directly in the initial hard scattering or from the decay of an excited charmonium state produced directly, and for J/ψ mesons coming from the decay of a long-lived b-hadron, either directly or via an excited charmonium state.

Nuclear effects are quantified by the nuclear modification factor, $R_{p\text{Pb}}$,

$$R_{p\text{Pb}}(p_T, y^*) \equiv \frac{1}{A} \frac{\mathrm{d}^2\sigma_{p\text{Pb}}(p_T, y^*)/\mathrm{d}p_T\mathrm{d}y^*}{\mathrm{d}^2\sigma_{pp}(p_T, y^*)/\mathrm{d}p_T\mathrm{d}y^*}, \quad (1)$$

where $A = 208$ is the mass number of the Pb ion, $\mathrm{d}^2\sigma_{p\text{Pb}}(p_T, y^*)/\mathrm{d}p_T\mathrm{d}y^*$ the J/ψ production cross-section in pPb or Pbp collisions and $\mathrm{d}^2\sigma_{pp}(p_T, y^*)/\mathrm{d}p_T\mathrm{d}y^*$ the J/ψ reference production cross-section in pp collisions at the same nucleon–nucleon centre-of-mass energy. The determination of the reference cross-section is described in Sec. 5.1. In the absence of nuclear effects, the nuclear modification factor is equal to unity.

In addition to the nuclear modification factor, the observable R_{FB} quantifies the relative forward-to-backward production rates. The forward-to-backward ratio is measured as the ratio of cross-sections in the positive and negative y^* acceptances evaluated in the same absolute y^* value ranges,

$$R_{\text{FB}}(p_T, y^*) \equiv \frac{\mathrm{d}^2\sigma_{p\text{Pb}}(p_T, +y^*)/\mathrm{d}p_T\mathrm{d}y^*}{\mathrm{d}^2\sigma_{p\text{Pb}}(p_T, -y^*)/\mathrm{d}p_T\mathrm{d}y^*}. \quad (2)$$

3. Event selection and cross-section determination

The J/ψ production cross-section measurement follows the approach described in Ref. [45]. The double differential J/ψ production cross-section in each kinematic bin of p_T and y^* is computed as

$$\frac{\mathrm{d}^2\sigma}{\mathrm{d}p_T\mathrm{d}y^*} = \frac{N(J/\psi \to \mu^+\mu^-)}{\mathcal{L} \times \epsilon_{\text{tot}} \times \mathcal{B}(J/\psi \to \mu^+\mu^-) \times \Delta p_T \times \Delta y^*}, \quad (3)$$

where $N(J/\psi \to \mu^+\mu^-)$ is the number of reconstructed prompt J/ψ or J/ψ-from-b-hadrons signal mesons, ϵ_{tot} is the total detection efficiency in the given kinematic bin, $\mathcal{B}(J/\psi \to \mu^+\mu^-) = (5.961 \pm 0.033)\%$ [46] is the branching fraction of the decay $J/\psi \to \mu^+\mu^-$, $\Delta p_T = 1$ GeV/c and $\Delta y^* = 0.5$ are the bin widths and $\mathcal{L}$ is the integrated luminosity. The luminosity is determined with a van der Meer scan, which was performed for both beam configurations. The luminosity determination follows closely the approach described in Ref. [47].

3.1. Selection

An online event selection is performed by a trigger system consisting of a hardware stage, which, for this analysis, selects events containing at least one muon with p_T larger than 500 MeV/c, followed by a software stage. In the first stage of the software trigger, two muon tracks with $p_T > 500$ MeV/c are required to form a J/ψ candidate with invariant mass $M_{\mu^+\mu^-} > 2.5$ GeV/c^2. In the second stage, J/ψ candidates with an invariant mass within 120 MeV/c^2 of the known value of the J/ψ mass [46] are selected.

In between the two software stages, the alignment and calibration of the detector is performed in near real-time [48]. The

same alignment and calibration is propagated to the offline reconstruction, ensuring consistent and high-quality particle identification (PID) information between the online and offline processings. The identical performance of the online and offline reconstructions offers the opportunity to perform physics analyses directly using candidates reconstructed in the trigger [49,50] as well as storing all reconstructed particles in the event [51]. The present analysis exploits this feature for the first time in proton-lead collisions and is using the online reconstruction.

At the analysis stage, each event is required to have at least one PV reconstructed from at least four tracks measured in the vertex detector. For events with multiple PVs, the PV that has the smallest χ_{IP}^2 with respect to the J/ψ candidate is chosen. Here, χ_{IP}^2 is defined as the difference between the vertex-fit χ^2 calculated with the J/ψ meson candidate included in or excluded from the PV fit. Each identified muon track is required to have $p_T > 750$ MeV/c, $2 < \eta < 5$ and to have a good-quality track fit. The two muon tracks of the J/ψ candidate must form a good-quality vertex, representing a tighter selection compared to the software trigger requirement.

3.2. Determination of signal yields

The reconstructed vertex of the J/ψ mesons originating from b-hadron decays tends to be separated from the PVs. These J/ψ mesons can thus be distinguished from prompt J/ψ mesons by exploiting the pseudo proper time defined as

$$t_z \equiv \frac{(z_{J/\psi} - z_{\text{PV}}) \times M_{J/\psi}}{p_z}, \qquad (4)$$

where $z_{J/\psi}$ and z_{PV} are the coordinates along the beam axis of the J/ψ decay vertex position and of the PV position, p_z is the z component of the J/ψ momentum and $M_{J/\psi}$ the known J/ψ mass. The yields of J/ψ signal candidates, for the prompt and J/ψ-from-b-hadrons categories, are determined from a simultaneous two-dimensional unbinned maximum likelihood fit to their invariant mass and pseudo proper time distributions, performed independently for each (p_T, y^*) bin.

In the fit function, the invariant-mass distribution of the signal is described by a Crystal Ball function [52], and the combinatorial background by an exponential function. The t_z distribution of prompt J/ψ is described by a Dirac δ-function $\delta(t_z)$, and that of J/ψ-from-b-hadrons by an exponential function for $t_z > 0$. Both of them are convolved with a triple-Gaussian resolution function, modelled from simulation samples to take into account the vertex resolution. The background t_z distribution is described by an empirical function derived from the shape observed in the J/ψ upper mass sideband, $3200 < M_{\mu^+\mu^-} < 3250$ MeV/c^2. This background comes from muons of semileptonic b- and c-hadron decays and from pions and kaons decaying in the detector. The distribution is parameterised as a sum of a Dirac δ-function and of five exponential functions, three for positive t_z values and two for negative t_z values, convolved with the sum of two Gaussian functions. An example of the invariant mass and the pseudo proper time distributions for one (p_T, y^*) bin is shown in Fig. 1 for the pPb and Pbp samples, where the one-dimensional projections of the fit result are drawn on the distributions. The width of the Gaussian part of the Crystal Ball function varies as a function of p_T between 10 MeV/c^2 (15 MeV/c^2) and 15 MeV/c^2 (33 MeV/c^2) in the lowest (highest) rapidity bins in the laboratory frame in both beam configurations. Due to the rapidity shifts between the laboratory frame and the nucleon–nucleon centre-of-mass frames, the two examples do not correspond to the same rapidity range in the laboratory while they are in the same $|y^*|$ range and, in this example, the mass resolution in the Pbp configuration is different from the one in the pPb configuration.

3.3. Efficiencies

The total detection efficiency, ϵ_{tot}, is the product of the geometrical acceptance, and the efficiencies for charged track reconstruction, particle identification, candidate and trigger selections. Samples of simulated events are used to evaluate these efficiencies except for the particle identification, which is determined in a data-driven approach. In the simulation, pPb and Pbp minimum-bias collisions are generated using the Epos event generator tuned with the LHC model [53]. The $J/\psi \to \mu^+\mu^-$ signal candidates are generated separately, with the Pythia8 generator [54] in pp collisions with beams having momenta equal to the momenta per nucleon of the p and Pb beams. They are then merged with the Epos minimum bias collisions to build the samples out of which the efficiencies are computed. The decays of hadrons are generated by EvtGen [55], in which final-state electromagnetic radiation is generated with Photos [56]. The interaction of the particles with the detector, and the detector response, are implemented using the Geant4 toolkit [57] as described in Ref. [58].

The charged-track reconstruction efficiency is first evaluated in simulation and is corrected using a data-driven tag-and-probe approach. For this purpose, J/ψ candidates are formed with one fully-reconstructed "tag" track and one "probe" track reconstructed partially with a subset of the tracking sub-detectors and both identified as muons [59] in data and in simulation. The ratio of the single track efficiencies from this tag-and-probe approach is used as a correction factor. These correction factors for each track are then applied to the signal candidates in the simulation to obtain the integrated efficiency in every kinematic bin. The tag-and-probe correction evaluation is relying on the pPb and the Pbp data samples, since the larger tracking calibration samples in pp collisions are limited in detector occupancy by an additional selection criterion on trigger level.

The muon identification efficiency is determined for each track in data with a tag-and-probe method [60] taking into account the efficiency variations as function of track momentum, pseudorapidity and detector occupancy. Calibration samples of J/ψ mesons are selected applying a tight identification criterion on one of the muons and no identification requirements to the second muon. However, the sizes of the calibration samples collected in pPb and Pbp collisions are limited. The efficiency is thus evaluated using the calibration samples collected in pp collisions, taking into account the different detector occupancies between pp, pPb and Pbp collisions, since this parameter affects the muon identification performance. The J/ψ simulation is weighted with the efficiencies determined per track in data in order to compute the muon identification efficiency in bins of J/ψ p_T and y^*.

The hardware and software trigger efficiencies obtained from the simulation are validated by comparing them with the efficiencies measured in control data samples recorded with minimum and unbiased trigger requirements, and containing J/ψ candidates.

The total efficiency in each (p_T, y^*) bin, ϵ_{tot}, is found to be the same for prompt J/ψ and J/ψ-from-b-hadrons within uncertainties and is taken to be identical for the two components. It is shown in Fig. 2 for pPb and Pbp collision data, as a function of the J/ψ p_T in the different rapidity bins. The uncertainties are the quadratic sums of the statistical uncertainties and the uncertainties associated to the data-driven corrections and validations, described in the following section.
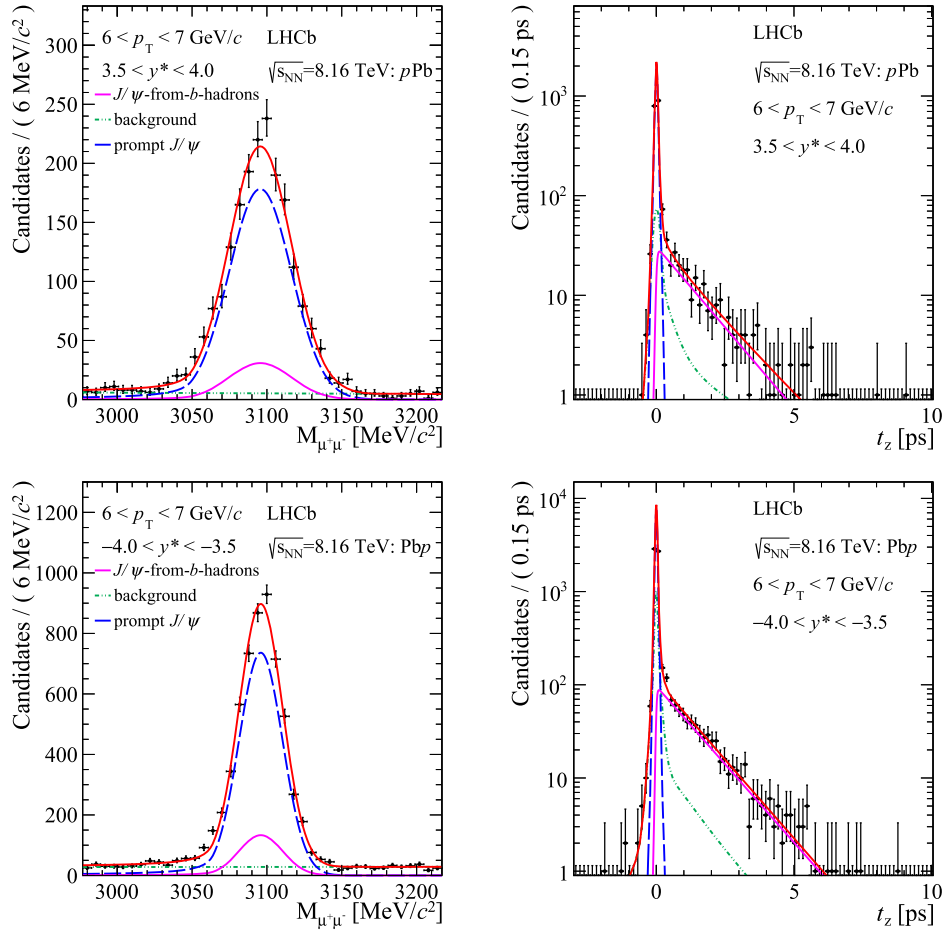
Fig. 1. (left) Invariant mass and (right) pseudo proper time distributions for J/ψ candidates in the bin $6 < p_T < 7$ GeV/c and $3.5 < |y^*| < 4.0$ for the (top) pPb and (bottom) Pbp samples respectively. The black circles with error bars represent the LHCb data. The projection of the result of the fit described in the text is drawn on each distribution: the red solid line is the total fit function, the blue dashed line is the prompt J/ψ signal component, the purple solid line is the J/ψ-from-b-hadrons signal component and the green dashed line is the combinatorial background component.
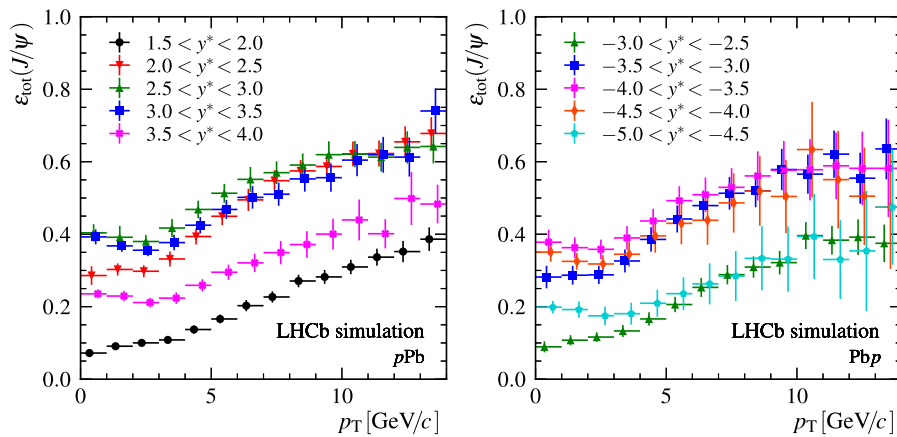
Fig. 2. Total J/ψ detection efficiency, ϵ_{tot}, as a function of the J/ψ p_T in different y^* bins for (left) pPb and (right) Pbp.

4. Systematic uncertainties

The systematic uncertainties on the cross-section of prompt J/ψ and J/ψ-from-b-hadrons are summarised in Table 1 and described in the following. The total detection efficiency ϵ_{tot} for prompt J/ψ and J/ψ-from-b is found to be equal within the

statistical precision of the simulation and all systematic uncertainties apply both for prompt J/ψ and J/ψ-from-b. Acceptance and reconstruction efficiencies of the J/ψ vector meson depend on its polarisation at production. The ALICE and the LHCb measurements in pp collisions [61,62] indicate a polarisation consistent with zero in most of the kinematic region of the analysis pre-
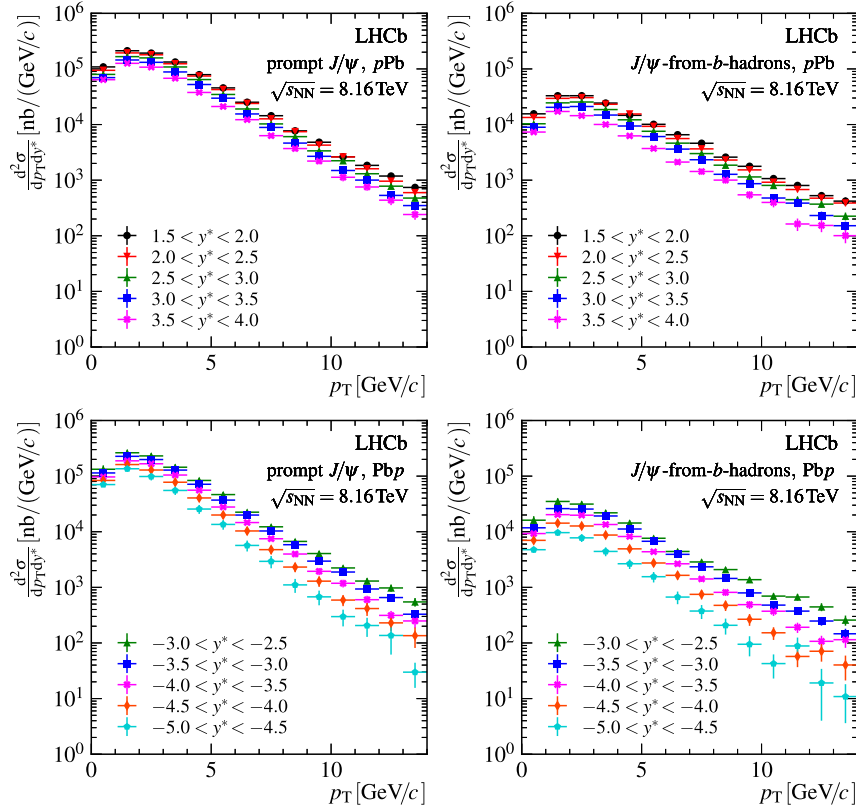
Fig. 3. Production cross-section for (top left) prompt J/ψ in pPb, (top right) J/ψ-from-b-hadrons in pPb, (bottom left) prompt J/ψ in Pbp and (bottom right) J/ψ-from-b-hadrons in Pbp. The data points are placed at the centre of the p_T bins, the horizontal error bars indicate the bin widths and the vertical error bars the total uncertainties, calculated as quadratic sums of the statistical and systematic uncertainties.

Table 1

Summary of relative systematic uncertainties in pPb and Pbp on the cross-section of prompt J/ψ and J/ψ-from-b-hadrons. Uncertainties that are computed bin-by-bin are expressed as ranges giving the minimum to maximum values. The last column indicates the correlation between bins within the same beam configuration.

Source	pPb	Pbp	Comment
Signal model	1.3%	1.3%	correlated
Muon identification	2.0%–11.0%	2.1%–15.3%	correlated
Tracking	3.0%–8.0%	5.9%–26.5%	correlated
Hardware trigger	1.0%–10.9%	1.0%–7.4%	correlated
Software trigger	2.0%	2.0%	correlated
Simulation statistics	0.4%–7.0%	0.4%–26.2%	uncorrelated
$\mathcal{B}(J/\psi \to \mu^+\mu^-)$	0.05%	0.05%	correlated
Luminosity	2.6%	2.5%	correlated
Polarisation	–	–	not considered

sented in this letter. In this analysis, it is assumed that the J/ψ mesons are produced with no polarisation in pPb and Pbp collisions at $\sqrt{s_{NN}} = 8.16$ TeV. No systematic uncertainty is assigned for the effects of polarisation.

The uncertainty on the J/ψ-meson yields, related to the modelling of the signal mass shape in the simultaneous mass and t_z fit, is studied using an alternative fit model. In this model, the signal mass shape is described by the sum of a Crystal Ball function and of a Gaussian function. The relative difference of the signal yields between the nominal and alternative fits amounts to 1.3%, which is taken as a fully correlated systematic uncertainty between bins. The uncertainty associated to the shape of the t_z distribution is negligible.

The uncertainty on the muon identification has multiple contributions. The statistical uncertainty of the efficiencies is derived from the calibration sample. The impact of the finite binning in muon momentum, pseudorapidity and detector occupancy on the

efficiencies is estimated by varying the binning scheme. Finally, an uncertainty due to the method to determine the number of signal candidates in the calibration samples is also considered. The total systematic uncertainty due to these three sources varies between 2% and 15%. It is assumed to be fully correlated between bins. This assumption is valid for neighbouring bins in acceptance. The bias introduced by this assumption in the evaluation of the total systematic uncertainty on integrated quantities is negligible.

The data-driven corrections to the track reconstruction efficiency carry uncertainties related to the statistical uncertainties of the data, dominating in most bins. In addition, a systematic uncertainty is related to a potential bias of the selection criteria which are necessary to obtain a good signal over background ratio for the determination of the efficiency corrections. A systematic uncertainty related to the method is applied similarly to pp collisions and amounts to 0.8% per track [59]. The total uncertainty related to charged track reconstruction varies from 3.0% to 8.0% for pPb and 5.9% to 26.5% for Pbp, correlated between bins. The uncertainty in the Pbp case is larger due to the smaller signal over background ratio for the partially reconstructed candidates used in the data-driven tag-and-probe method compared to the pPb case. The assumption on the correlation is valid for neighbouring bins. The introduced bias in the evaluation of the total systematic uncertainty on integrated quantities is negligible. The largest uncertainties appear at low track momenta and hence low J/ψ p_T.

The trigger efficiency is determined in data and in simulation by the data-driven method described in the previous section and in Ref. [49]. The uncertainties related to the trigger are estimated by comparing the results in simulation and in data. The uncertainty on the hardware trigger efficiency is found to vary between 1% and 11%, and the uncertainty on the software trigger efficiency is

estimated to amount to 2%. The trigger uncertainties are assumed to be fully correlated between bins.

The finite size of the simulation event sample used for the efficiency determination introduces a systematic uncertainty, which varies between 0.4% and 26.2% between the kinematic bins of the pPb and the Pbp simulation. The largest relative values appear at high p_T and large rapidities and do not dominate the overall uncertainties. They differ between the pPb and Pbp case due to the different rapidity coverage in the centre-of-mass system. The branching fraction contributes to the cross-section uncertainty with 0.05%. The luminosity measurement uncertainty amounts to 2.6% in pPb and to 2.5% in Pbp collisions. The uncertainty on all other applied selections is found to be negligible based on comparisons between data and simulation signal distributions of selection and kinematics variables.

5. Results

5.1. Cross-sections

The measured double-differential cross-sections of prompt J/ψ and J/ψ-from-b-hadrons in the pPb and Pbp data samples are shown in Fig. 3, as a function of p_T for the considered y^* bins. The numerical values are presented in Appendices A.1–A.4. The total cross-sections, integrated over the measurement ranges, amount to

$$\sigma_{\text{prompt } J/\psi}(1.5 < y^* < 4.0, \ p_T < 14 \text{ GeV}/c)$$
$$= 1625 \pm 4 \pm 117 \, \mu b,$$

$$\sigma_{J/\psi\text{-from-}b\text{-hadrons}}(1.5 < y^* < 4.0, \ p_T < 14 \text{ GeV}/c)$$
$$= 276 \pm 2 \pm \ 20 \, \mu b,$$

$$\sigma_{\text{prompt } J/\psi}(-5.0 < y^* < -2.5, \ p_T < 14 \text{ GeV}/c)$$
$$= 1692 \pm 4 \pm 182 \, \mu b,$$

$$\sigma_{J/\psi\text{-from-}b\text{-hadrons}}(-5.0 < y^* < -2.5, \ p_T < 14 \text{ GeV}/c)$$
$$= 209 \pm 1 \pm \ 22 \, \mu b,$$

where the first uncertainties are statistical and the second systematic.

The fraction of J/ψ-from-b-hadrons, f_b, is derived from the cross-section measurements. The fraction f_b is defined as

$$f_b(p_T, y^*) \equiv \tag{5}$$
$$\frac{\mathrm{d}^2\sigma_{J/\psi\text{-from-}b\text{-hadrons}}/\mathrm{d}p_T\mathrm{d}y^*}{\mathrm{d}^2\sigma_{\text{prompt } J/\psi}/\mathrm{d}p_T\mathrm{d}y^* + \mathrm{d}^2\sigma_{J/\psi\text{-from-}b\text{-hadrons}}/\mathrm{d}p_T\mathrm{d}y^*}.$$

Most of the systematic uncertainties cancel in the determination of f_b, which can thus be measured precisely. The values of f_b as a function of p_T in the different y^* bins are shown in Fig. 4 for pPb and Pbp and listed in Appendices A.5 and A.6. The values of f_b measured in pp collisions at a centre-of-mass energy of 8 TeV [63], are shown on the same figure for comparison. The differences that appear between the measurements performed in the two collision systems indicate, particularly at low p_T, different nuclear modifications for prompt J/ψ and b-quark production.

The focus of this publication is the quantification of the nuclear effects, comparing in particular the J/ψ production in proton-lead collisions with that in pp collisions at the same energy. Following the same approach as in the previous LHCb publication on J/ψ production in pPb collisions at $\sqrt{s_{NN}} = 5$ TeV [27], a pp reference cross-section at $\sqrt{s} = 8.16$ TeV is determined from an interpolation of the LHCb cross-section measurements at 7 TeV [64], 8 TeV [63] and 13 TeV [45]. The extracted reference cross-section is in agreement with the measured cross-section at $\sqrt{s} = 8$ TeV. For
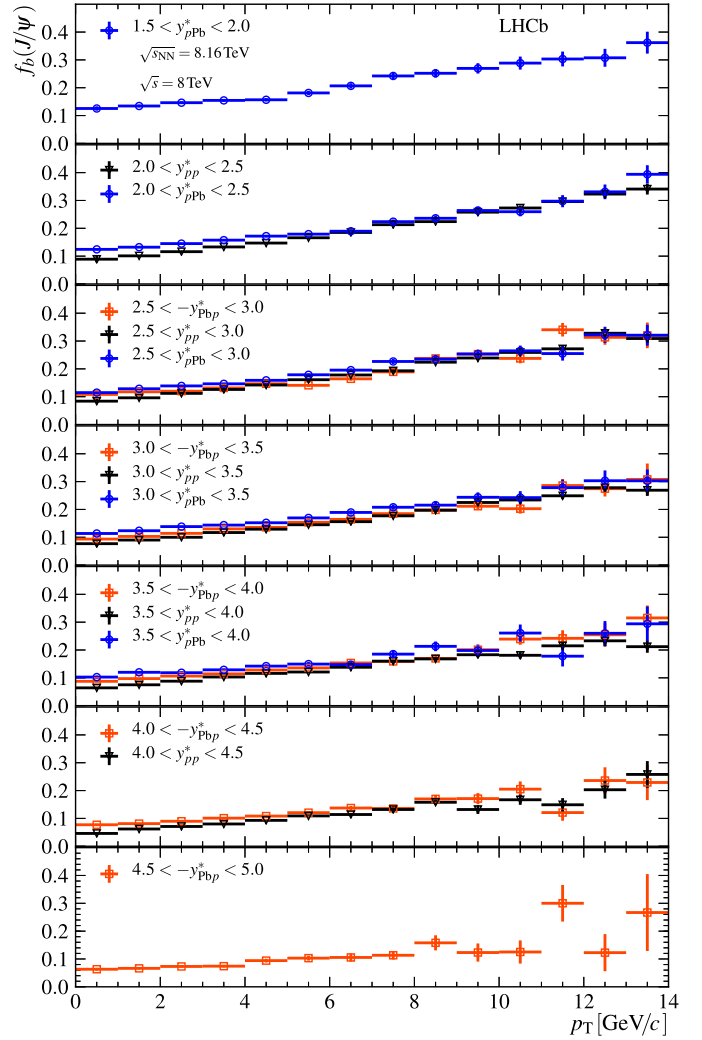
Fig. 4. Fraction of J/ψ-from-b-hadrons, f_b, as a function of p_T for (from top to bottom) $1.5 < |y^*| < 2.0$, $2.0 < |y^*| < 2.5$, $2.5 < |y^*| < 3.0$, $3.0 < |y^*| < 3.5$, $3.5 < |y^*| < 4.0$, $4.0 < |y^*| < 4.5$ and $4.5 < |y^*| < 5.0$. The data points are placed at the centre of the p_T bins, the horizontal error bars indicate the bin widths and the vertical error bars the total uncertainties, calculated as quadratic sums of the statistical and systematic uncertainties. Blue circles are for pPb collisions, red squares for Pbp collisions and black triangles for pp collisions at 8 TeV taken from Ref. [63].

the edges of the rapidity range in pPb collisions ($1.5 < y^* < 2.0$) and in Pbp collisions ($4.5 < y^* < 5.0$), which are not covered by the measurements in pp collisions, an extrapolation is used based on the experimental measurements. The interpolation and the extrapolation methods were validated with ALICE and LHCb data and are described in Ref. [65].

The cross-section as a function of y^*, integrated over p_T in the range $0 < p_T < 14$ GeV/c in pPb and Pbp collisions, is shown in Fig. 5. The cross-section is compared with the reference cross-section for prompt J/ψ and J/ψ-from-b-hadrons production in pp collisions at $\sqrt{s} = 8.16$ TeV, multiplied by the Pb mass number $A = 208$. The total relative uncertainties on the pp cross-section range between 3% and 11% and are largest in the bins based on extrapolations. The cross-sections as a function of p_T, integrated over the range $1.5 < y^* < 4.0$ for pPb and $-5.0 < y^* < -2.5$ for Pbp, and the corresponding scaled pp cross-sections are represented in Fig. 6. In this case, the total relative uncertainties on the pp reference cross-section vary between 3% and 18%.
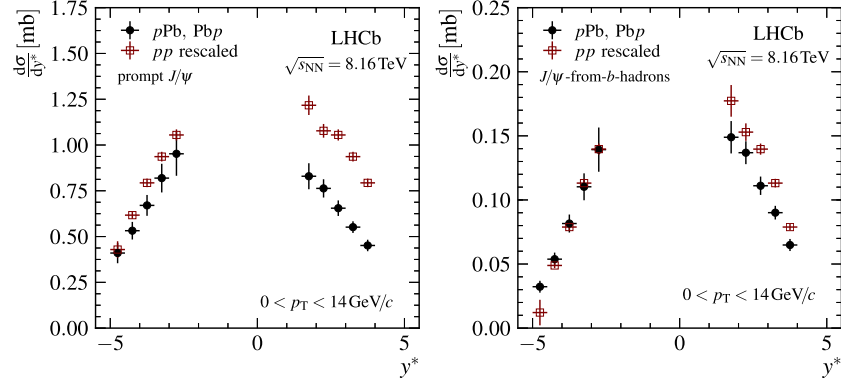
Fig. 5. Absolute production cross-sections of (left) prompt J/ψ and (right) J/ψ-from-b-hadrons, as a function of y^*, integrated over the range $0 < p_T < 14$ GeV/c. The black circles are the pPb and Pbp values and the red open squares the values for pp collisions at the same energy, multiplied by the Pb mass number $A = 208$. The horizontal error bars are the bin widths and vertical error bars the total uncertainties.
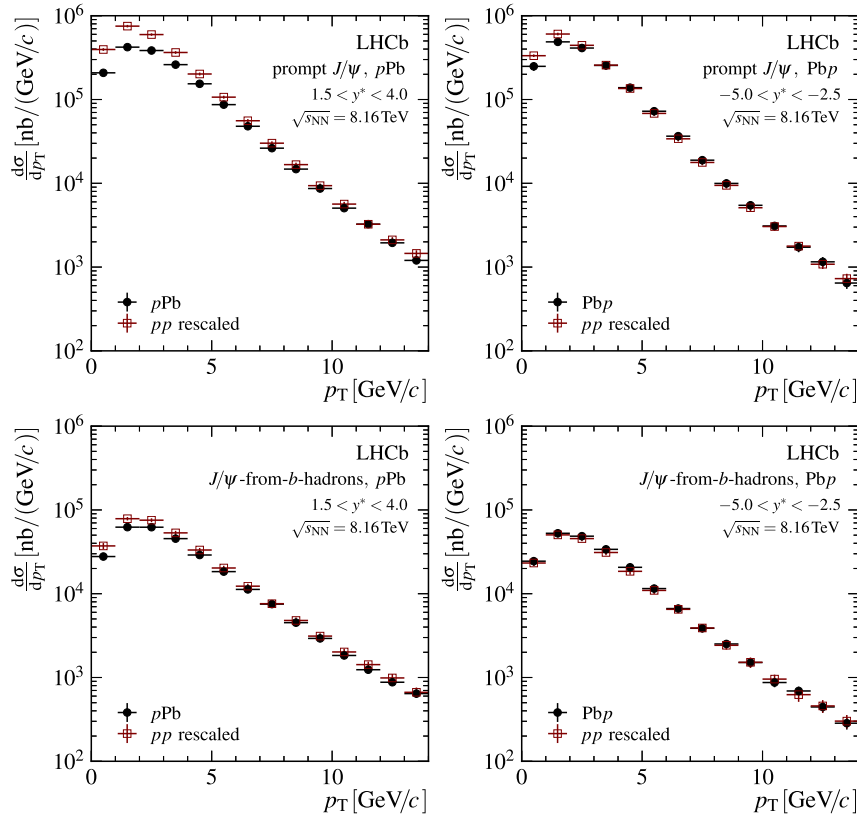
Fig. 6. Absolute production cross-sections of (top left) prompt J/ψ in pPb, (top right) prompt J/ψ in Pbp, (bottom left) J/ψ-from-b-hadrons in Pbp and (bottom left) J/ψ-from-b-hadrons in Pbp, as a function of p_T and integrated over the rapidity range of the analysis. The black circles are the pPb and Pbp values and the red open squares the values for pp collisions at the same energy, multiplied by the Pb mass number $A = 208$, integrated over the same rapidity ranges. The horizontal error bars are the bin widths and vertical error bars the total uncertainties.

5.2. Nuclear modification factors

The nuclear modification factor $R_{p\text{Pb}}$ defined in Eq. (1) is computed from the prompt J/ψ and J/ψ-from-b-hadrons production cross-sections in pp and pPb or Pbp collisions. The systematic uncertainties are assumed to be uncorrelated between the measurements in proton-lead and in pp collisions. The nuclear modification factors for prompt J/ψ and J/ψ-from-b-hadrons production as functions of p_T or y^*, integrating over the other variable, are shown in Figs. 7 and 8, respectively. The numerical values are

available in Appendix B. The results at $\sqrt{s_{NN}} = 5$ TeV [27] are also depicted on Fig. 8 and are in good agreement with the new and more precise results at $\sqrt{s_{NN}} = 8.16$ TeV.

At forward rapidity, $1.5 < y^* < 4.0$, a strong suppression of up to 50% is observed in the case of prompt J/ψ production at low p_T (Fig. 7). This behaviour results in a strong suppression in the nuclear modification factor as a function of rapidity shown in Fig. 8. With increasing p_T, $R_{p\text{Pb}}$ approaches unity and the suppression is stronger at more forward rapidities. The production of J/ψ-from-b-hadrons is also suppressed compared to
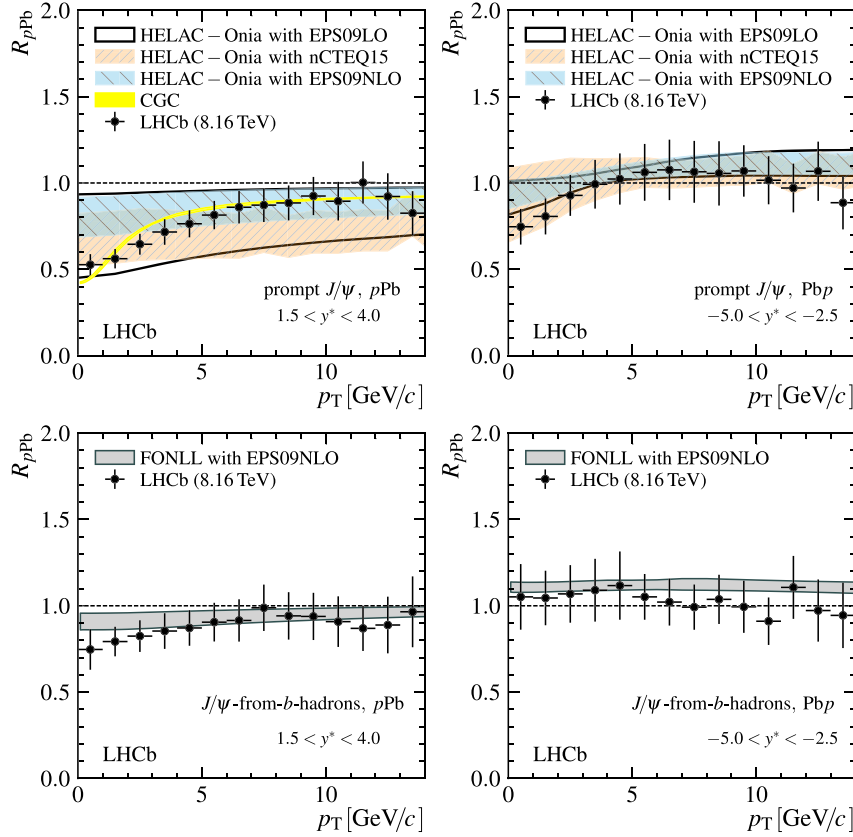
Fig. 7. J/ψ nuclear modification factor, $R_{p\mathrm{Pb}}$, integrated over y^* in the analysis range, as a function of p_T for (top left) prompt J/ψ in pPb, (bottom left) J/ψ-from-b-hadrons in pPb, (top right) prompt J/ψ in Pbp and (bottom right) J/ψ-from-b-hadrons in Pbp. Horizontal error bars are the bin widths, vertical error bars the total uncertainties. The black circles are the values measured in this letter and the coloured areas the theoretical predictions from the models detailed in the text with their uncertainties.
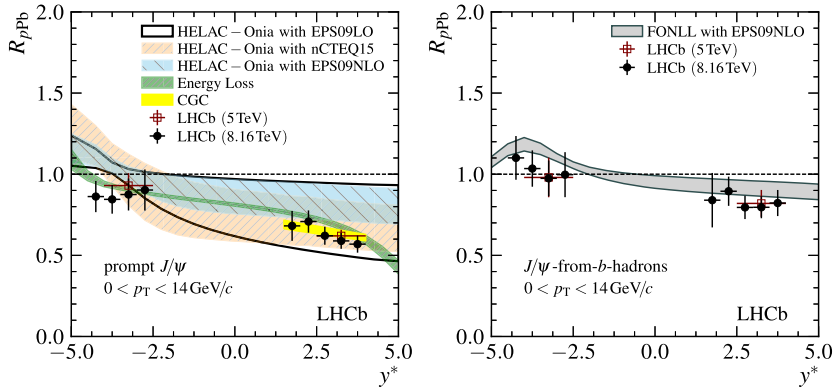
Fig. 8. J/ψ nuclear modification factor, $R_{p\mathrm{Pb}}$, integrated over p_T in the range $0 < p_T < 14$ GeV/c, as a function of y^* for (left) prompt J/ψ and (right) J/ψ-from-b-hadrons. The horizontal error bars are the bin widths and vertical error bars the total uncertainties. The black circles are the values measured in this letter, the red squares the values measured at $\sqrt{s_{NN}} = 5$ TeV from Ref. [27] and the coloured areas the theoretical computations from the models detailed in the text, with their uncertainties.

that in pp collisions at forward rapidities, although to a lesser degree, as shown in Fig. 8. No dependence as a function of rapidity can be observed within the experimental uncertainties. The dependence as a function of the transverse momentum is weaker for J/ψ-from-b-hadrons compared to prompt J/ψ, but the nuclear modification factor is also approaching unity at high transverse momentum.

At backward rapidity, $-5.0 < y^* < -2.5$, a weaker suppression of prompt J/ψ production at low p_T is observed, of up to 25%. Similarly to the forward-rapidity region, the suppression is weak-

ening and the nuclear modification factor is approaching values consistent with unity at high transverse momentum. The nuclear modification factor as a function of rapidity shows a weak suppression with no visible rapidity dependence within experimental uncertainties. The nuclear modification factor of J/ψ-from-b-hadrons at backward rapidity is consistent with unity over the full kinematic region.

The measurements of prompt J/ψ nuclear modification factors are compared in Figs. 7 and 8 with three groups of calculations:

1. collinear factorisation using different nPDFs [66,67] (labelled "HELAC-Onia with EPS09LO", "HELAC-Onia with nCTEQ15" and "HELAC-Onia with EPS09NLO" on the figures),
2. CGC effective field theory in the dilute-dense approximation taking into account the dense nature of the Pb nucleus, but approximating the proton as a dilute parton source [24,68] (labelled "CGC"),
3. coherent energy loss calculating the impact of low angle coherent gluon radiation during the crossing of the nucleus [25] (labelled "Energy Loss").

The CGC calculations [24,68] describe well the behaviour of the prompt J/ψ data at forward rapidity. At backward rapidity, this approach is not available due to the breakdown of the dilute approximation for the partons in the proton. The uncertainties take into account the variation of the charm-quark mass and the factorisation scale. These uncertainties largely cancel in this ratio of cross-sections. The collinear calculations are based on the HELAC-Onia event generator [66,67], tuned to reproduce prompt J/ψ cross-section measurements in pp collision [21] and combined with different sets of nPDFs: nCTEQ15 [14] and EPS09 at leading (LO) and at next-to-leading order (NLO) [12]. However, the large uncertainties reveal the missing experimental constraints on the gluon density in the nucleus at low x probed by the measurements in the LHCb detector acceptance. At backward rapidities, the experimental points are found at the lower bound or slightly below the theoretical uncertainty bands and exhibit a different rapidity shape from the calculations. The coherent energy loss model [25] is able to provide the overall shape of the suppression, but overestimates the experimental data at forward rapidities. The uncertainty of this calculation reflects the allowed variation of the parameterisation of pp data used in the model and the allowed variation of the only free model parameter from fits to other measurements.

The measurements of J/ψ-from-b-hadrons nuclear modification factors are compared in Figs. 7 and 8 with a perturbative QCD calculation at fixed-order next-to-leading-logarithms (FONLL) [69, 70] coupled with the EPS09 nPDF set at next-to-leading order [12] (labelled "FONLL with EPS09NLO" on the figures). The displayed uncertainties correspond to the uncertainties from the nPDF, which are of similar size to or smaller than the total experimental uncertainties. The $p_{\rm T}$ dependence of the experimental data is described within uncertainties by the model. However, the calculation tends to show larger nuclear modification factors than the data. This tendency is confirmed by the nuclear modification factor as a function of rapidity, where the most precise experimental data points are below the model uncertainty band. Furthermore, at backward rapidity, the slope of the theoretical curve is not seen in the experimental data.

Finally, recent measurements have shown that long-range collective effects, which have previously been observed in relatively large nucleus–nucleus collision systems, may also be present in smaller collision systems at large charged-particle multiplicites [71–74]. If these effects have a hydrodynamic origin, momentum anisotropies at the quark level can arise and may modify the distribution of observed heavy-quark hadrons [75]. However, the expected magnitude of these effects on prompt J/ψ or J/ψ-from-b-hadrons production has not yet been calculated. Since the measurements in this letter are integrated over charged-particle multiplicity, potential modifications in high-multiplicity events are diluted.

5.3. Forward-to-backward ratios

Figs. 9 and 10 show the forward-to-backward ratio, $R_{\rm FB}$, of the production of prompt J/ψ and J/ψ-from-b-hadrons, in the overlapping acceptance between the two beam configurations, as functions of transverse momentum and rapidity, respectively. The numerical results are listed in Appendix C. In the $R_{\rm FB}$ ratio, most of the systematic uncertainties cancel. The measurements of $R_{\rm FB}$ at $\sqrt{s_{NN}} = 5$ TeV [27] are compared with the measurements at 8.16 TeV and are found to be in agreement. They are compared with the theoretical computations based on collinear factorisation with different nPDFs described in the previous section.

The calculations with different nPDFs do not fully cover the experimental points within uncertainties in particular at low $p_{\rm T}$ with the exception of the EPS09LO combination, which has considerably larger uncertainties. However, a detailed analysis of theoretical correlations in the $p_{\rm T}$-dependent $R_{\rm FB}$ may be interesting for future studies in order to quantify more precisely the discrepancies. The coherent energy loss calculation is compared with the rapidity dependence of the experimental data points in Fig. 10. It shows within its small uncertainties a slightly different slope from the experimental data points and predicts larger values in the bin at smallest $|y^*|$.

The $R_{\rm FB}$ ratio of J/ψ-from-b-hadrons in Fig. 9 shows a rising trend as a function of transverse momentum starting from a value 0.7 at low $p_{\rm T}$ towards values consistent with unity at high $p_{\rm T}$. The rapidity dependence of $R_{\rm FB}$ in Fig. 10 is consistent with a flat behaviour with a central value of 0.8.

6. Conclusions

The differential production cross-sections of prompt J/ψ and J/ψ-from-b-hadrons in pPb and Pbp collisions at $\sqrt{s_{NN}} = 8.16$ TeV are measured in the range $0 < p_{\rm T} < 14$ GeV/c. The nuclear modification factors are similar to the findings at a collision energy of $\sqrt{s_{NN}} = 5$ TeV, but with increased precision thanks to 10 and 40 times larger data sets in pPb and Pbp collisions, respectively. A suppression of prompt J/ψ production compared to pp collisions of up to 50% (25%) in pPb (Pbp) at the lowest transverse momentum is observed. In both configurations, the nuclear modification factor approaches unity asymptotically at the highest $p_{\rm T}$. Theoretical calculations for the nuclear modification factor based on collinear factorisation with different nuclear parton distribution functions, coherent energy loss as well as the colour glass condensate model can account for the majority of the observed dependences. For the first time, beauty-hadron production is measured precisely down to $p_{\rm T} = 0$ at the LHC in pPb and Pbp collisions. In pPb, a weak suppression at the lowest transverse momenta is observed, whereas in Pbp no significant deviation from unity in the nuclear modification factor is found. This weak modification of beauty production in proton-ion collisions is an important ingredient for the investigation of the modifications of beauty production in heavy-ion collisions. Although the presented measurements have improved precision, it is not possible to single out the main nuclear modification mechanism between different phenomenological approaches for charmonium production in proton-lead collisions at the TeV scale. This measurement of J/ψ production is the first step towards measurements of other charmonium states as well as complementary observables like Drell–Yan production, to improve the understanding of quantum chromodynamics at low x and in dense nuclear environments.

Acknowledgements
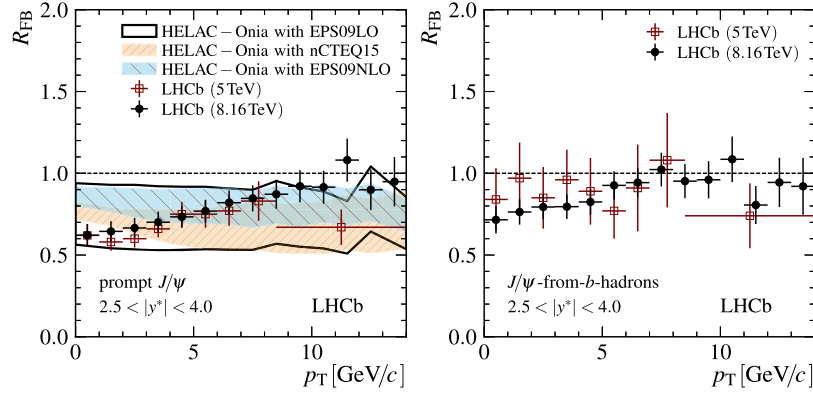
Fig. 9. Forward-to-backward ratios, R_{FB}, integrated over the common rapidity range $2.5 < |y^*| < 4.0$ as a function of p_T for (left) prompt J/ψ and (right) J/ψ-from-b-hadrons. The horizontal error bars are the bin widths and the vertical error bars the total uncertainties. The black circles are the values measured in this letter, the red squares the values measured at $\sqrt{s_{NN}} = 5$ TeV from Ref. [27] and the coloured areas the theoretical computations from the models detailed in the text, with their uncertainties.

Fig. 10. Forward-to-backward ratios, R_{FB}, integrated over p_T in the range $0 < p_T < 14$ GeV/c as a function of $|y^*|$ for (left) prompt J/ψ and (right) J/ψ-from-b-hadrons. The horizontal error bars are the bin widths and the vertical error bars the total uncertainties. The black circles are the values measured in this letter, the red squares the values measured at $\sqrt{s_{NN}} = 5$ TeV from Ref. [27] and the coloured areas the theoretical computations from the models detailed in the text, with their uncertainties.

Appendix A. Cross-section numerical results

A.1. $\frac{d^2\sigma}{dp_T dy^*}$ for prompt J/ψ in pPb

Table 2

Prompt J/ψ absolute production cross-section in pPb, as a function of p_T and y^*. The quoted uncertainties are the total uncertainties, and the breakdown into statistical uncertainties, and correlated and uncorrelated systematic uncertainties.

p_T bin (GeV/c)	y^* bin	$\frac{d^2\sigma}{dp_T dy^*}$ [nb/(GeV/c)]	stat.	corr.	uncorr.
$0 < p_T < 1$	$1.5 < y^* < 2.0$	$108\,700 \pm 16\,000$	2700	15\,700	1700
$0 < p_T < 1$	$2.0 < y^* < 2.5$	$94\,300 \pm 8\,900$	1400	8800	700
$0 < p_T < 1$	$2.5 < y^* < 3.0$	$79\,700 \pm 5\,400$	1100	5200	500
$0 < p_T < 1$	$3.0 < y^* < 3.5$	$69\,800 \pm 4\,300$	1000	4200	400
$0 < p_T < 1$	$3.5 < y^* < 4.0$	$64\,000 \pm 4\,100$	1100	3900	500
$1 < p_T < 2$	$1.5 < y^* < 2.0$	$212\,200 \pm 18\,100$	3300	17\,700	2000
$1 < p_T < 2$	$2.0 < y^* < 2.5$	$194\,000 \pm 12\,000$	2000	12\,000	1000
$1 < p_T < 2$	$2.5 < y^* < 3.0$	$166\,400 \pm 14\,300$	1500	14\,200	700
$1 < p_T < 2$	$3.0 < y^* < 3.5$	$144\,800 \pm 7\,900$	1400	7700	600
$1 < p_T < 2$	$3.5 < y^* < 4.0$	$126\,100 \pm 8\,800$	1500	8700	700
$2 < p_T < 3$	$1.5 < y^* < 2.0$	$192\,600 \pm 14\,800$	2800	14\,400	1900
$2 < p_T < 3$	$2.0 < y^* < 2.5$	$180\,000 \pm 11\,000$	2000	11\,000	1000
$2 < p_T < 3$	$2.5 < y^* < 3.0$	$157\,800 \pm 8\,900$	1400	8800	800
$2 < p_T < 3$	$3.0 < y^* < 3.5$	$131\,400 \pm 7\,300$	1300	7100	700
$2 < p_T < 3$	$3.5 < y^* < 4.0$	$107\,500 \pm 7\,600$	1400	7400	800

Table 2 (*Continued*)

p_T bin (GeV/c)	y^* bin	$\frac{d^2\sigma}{dp_T dy^*}$ [nb/(GeV/c)]	stat.	corr.	uncorr.
$3 < p_T < 4$	$1.5 < y^* < 2.0$	$133\,100 \pm 12\,200$	2100	11900	1500
$3 < p_T < 4$	$2.0 < y^* < 2.5$	$123\,800 \pm 8\,700$	1200	8600	800
$3 < p_T < 4$	$2.5 < y^* < 3.0$	$108\,500 \pm 7\,300$	1000	7200	600
$3 < p_T < 4$	$3.0 < y^* < 3.5$	$88\,200 \pm 5\,700$	900	5600	500
$3 < p_T < 4$	$3.5 < y^* < 4.0$	$67\,900 \pm 5\,300$	900	5200	600
$4 < p_T < 5$	$1.5 < y^* < 2.0$	$78\,800 \pm 6\,700$	1400	6500	1000
$4 < p_T < 5$	$2.0 < y^* < 2.5$	$74\,600 \pm 4\,800$	800	4700	500
$4 < p_T < 5$	$2.5 < y^* < 3.0$	$64\,400 \pm 3\,900$	700	3800	400
$4 < p_T < 5$	$3.0 < y^* < 3.5$	$52\,500 \pm 3\,200$	600	3200	400
$4 < p_T < 5$	$3.5 < y^* < 4.0$	$37\,700 \pm 2\,800$	700	2700	400
$5 < p_T < 6$	$1.5 < y^* < 2.0$	$45\,600 \pm 3\,700$	900	3500	700
$5 < p_T < 6$	$2.0 < y^* < 2.5$	$42\,500 \pm 2\,700$	500	2600	400
$5 < p_T < 6$	$2.5 < y^* < 3.0$	$34\,750 \pm 2\,080$	460	2010	280
$5 < p_T < 6$	$3.0 < y^* < 3.5$	$29\,790 \pm 1\,940$	440	1870	260
$5 < p_T < 6$	$3.5 < y^* < 4.0$	$21\,100 \pm 1\,680$	460	1600	250
$6 < p_T < 7$	$1.5 < y^* < 2.0$	$25\,200 \pm 2\,100$	600	2000	400
$6 < p_T < 7$	$2.0 < y^* < 2.5$	$23\,940 \pm 1\,680$	380	1620	250
$6 < p_T < 7$	$2.5 < y^* < 3.0$	$19\,050 \pm 1\,350$	320	1300	190
$6 < p_T < 7$	$3.0 < y^* < 3.5$	$15\,500 \pm 1\,110$	300	1050	170
$6 < p_T < 7$	$3.5 < y^* < 4.0$	$12\,230 \pm 1\,090$	340	1020	190

Table 3

Prompt J/ψ absolute production cross-section in pPb, as a function of p_T and y^*. The quoted uncertainties are the total uncertainties, and the breakdown into statistical uncertainties, and correlated and uncorrelated systematic uncertainties.

p_T bin (GeV/c)	y^* bin	$\frac{d^2\sigma}{dp_T dy^*}$ [nb/(GeV/c)]	stat.	corr.	uncorr.
$7 < p_T < 8$	$1.5 < y^* < 2.0$	$14\,410 \pm 1\,170$	440	1030	330
$7 < p_T < 8$	$2.0 < y^* < 2.5$	$12\,660 \pm 800$	260	740	160
$7 < p_T < 8$	$2.5 < y^* < 3.0$	$10\,260 \pm 680$	230	630	130
$7 < p_T < 8$	$3.0 < y^* < 3.5$	$8\,870 \pm 660$	230	600	130
$7 < p_T < 8$	$3.5 < y^* < 4.0$	$6\,310 \pm 660$	240	600	120
$8 < p_T < 9$	$1.5 < y^* < 2.0$	$7\,700 \pm 620$	290	500	210
$8 < p_T < 9$	$2.0 < y^* < 2.5$	$7\,440 \pm 490$	190	430	120
$8 < p_T < 9$	$2.5 < y^* < 3.0$	$6\,060 \pm 410$	170	360	100
$8 < p_T < 9$	$3.0 < y^* < 3.5$	$4\,640 \pm 360$	160	310	90
$8 < p_T < 9$	$3.5 < y^* < 4.0$	$3\,700 \pm 400$	200	400	100
$9 < p_T < 10$	$1.5 < y^* < 2.0$	$4\,810 \pm 420$	220	320	160
$9 < p_T < 10$	$2.0 < y^* < 2.5$	$4\,270 \pm 300$	140	240	90
$9 < p_T < 10$	$2.5 < y^* < 3.0$	$3\,360 \pm 260$	130	210	70
$9 < p_T < 10$	$3.0 < y^* < 3.5$	$2\,680 \pm 240$	120	190	70
$9 < p_T < 10$	$3.5 < y^* < 4.0$	$2\,200 \pm 280$	130	230	70
$10 < p_T < 11$	$1.5 < y^* < 2.0$	$2\,630 \pm 240$	160	150	100
$10 < p_T < 11$	$2.0 < y^* < 2.5$	$2\,620 \pm 200$	110	150	60
$10 < p_T < 11$	$2.5 < y^* < 3.0$	$2\,230 \pm 180$	100	130	60
$10 < p_T < 11$	$3.0 < y^* < 3.5$	$1\,490 \pm 150$	80	110	40
$10 < p_T < 11$	$3.5 < y^* < 4.0$	$1\,130 \pm 170$	90	140	40
$11 < p_T < 12$	$1.5 < y^* < 2.0$	$1\,840 \pm 190$	120	110	90
$11 < p_T < 12$	$2.0 < y^* < 2.5$	$1\,600 \pm 130$	90	90	50
$11 < p_T < 12$	$2.5 < y^* < 3.0$	$1\,300 \pm 120$	80	80	50
$11 < p_T < 12$	$3.0 < y^* < 3.5$	$1\,000 \pm 110$	70	80	40
$11 < p_T < 12$	$3.5 < y^* < 4.0$	750 ± 110	80	70	40
$12 < p_T < 13$	$1.5 < y^* < 2.0$	$1\,190 \pm 140$	100	80	70
$12 < p_T < 13$	$2.0 < y^* < 2.5$	958 ± 94	64	59	33
$12 < p_T < 13$	$2.5 < y^* < 3.0$	779 ± 82	58	49	31
$12 < p_T < 13$	$3.0 < y^* < 3.5$	531 ± 71	51	41	26
$12 < p_T < 13$	$3.5 < y^* < 4.0$	436 ± 80	47	61	21
$13 < p_T < 14$	$1.5 < y^* < 2.0$	740 ± 100	70	40	50
$13 < p_T < 14$	$2.0 < y^* < 2.5$	596 ± 65	49	34	25
$13 < p_T < 14$	$2.5 < y^* < 3.0$	476 ± 59	45	27	24
$13 < p_T < 14$	$3.0 < y^* < 3.5$	349 ± 47	35	27	15
$13 < p_T < 14$	$3.5 < y^* < 4.0$	241 ± 47	38	21	16

A.2. $\frac{d^2\sigma}{dp_T dy^*}$ *for* J/ψ-*from-b-hadrons in* pPb

Table 4

J/ψ-from-b-hadrons absolute production cross-section in pPb, as a function of p_T and y^*. The quoted uncertainties are the total uncertainties, and the breakdown into statistical uncertainties, and correlated and uncorrelated systematic uncertainties.

p_T bin (GeV/c)	y^* bin	$\frac{d^2\sigma}{dp_T dy^*}$ [nb/(GeV/c)]	stat.	corr.	uncorr.
$0 < p_T < 1$	$1.5 < y^* < 2.0$	$15\,580 \pm 2\,480$	1020	2250	240
$0 < p_T < 1$	$2.0 < y^* < 2.5$	$13\,400 \pm 1\,300$	500	1300	100
$0 < p_T < 1$	$2.5 < y^* < 3.0$	$10\,320 \pm 780$	370	680	60
$0 < p_T < 1$	$3.0 < y^* < 3.5$	$8\,940 \pm 640$	350	540	50
$0 < p_T < 1$	$3.5 < y^* < 4.0$	$7\,330 \pm 600$	400	440	60
$1 < p_T < 2$	$1.5 < y^* < 2.0$	$32\,950 \pm 3\,050$	1290	2740	320
$1 < p_T < 2$	$2.0 < y^* < 2.5$	$29\,550 \pm 1\,980$	670	1850	150
$1 < p_T < 2$	$2.5 < y^* < 3.0$	$24\,530 \pm 2\,170$	540	2100	110
$1 < p_T < 2$	$3.0 < y^* < 3.5$	$20\,390 \pm 1\,200$	510	1090	90
$1 < p_T < 2$	$3.5 < y^* < 4.0$	$17\,180 \pm 1\,330$	600	1180	100
$2 < p_T < 3$	$1.5 < y^* < 2.0$	$32\,980 \pm 2\,740$	1160	2460	320
$2 < p_T < 3$	$2.0 < y^* < 2.5$	$30\,480 \pm 2\,010$	650	1900	170
$2 < p_T < 3$	$2.5 < y^* < 3.0$	$25\,420 \pm 1\,520$	530	1420	120
$2 < p_T < 3$	$3.0 < y^* < 3.5$	$21\,100 \pm 1\,260$	500	1150	110
$2 < p_T < 3$	$3.5 < y^* < 4.0$	$14\,440 \pm 1\,140$	550	1000	100
$3 < p_T < 4$	$1.5 < y^* < 2.0$	$24\,320 \pm 2\,370$	900	2180	280
$3 < p_T < 4$	$2.0 < y^* < 2.5$	$23\,150 \pm 1\,690$	510	1600	140
$3 < p_T < 4$	$2.5 < y^* < 3.0$	$18\,590 \pm 1\,300$	410	1230	100
$3 < p_T < 4$	$3.0 < y^* < 3.5$	$14\,810 \pm 1\,030$	390	940	90
$3 < p_T < 4$	$3.5 < y^* < 4.0$	$10\,030 \pm 860$	390	760	80
$4 < p_T < 5$	$1.5 < y^* < 2.0$	$14\,650 \pm 1\,370$	620	1210	190
$4 < p_T < 5$	$2.0 < y^* < 2.5$	$15\,480 \pm 1\,050$	380	970	110
$4 < p_T < 5$	$2.5 < y^* < 3.0$	$12\,160 \pm 790$	300	720	80
$4 < p_T < 5$	$3.0 < y^* < 3.5$	$9\,410 \pm 640$	290	570	70
$4 < p_T < 5$	$3.5 < y^* < 4.0$	$6\,250 \pm 540$	310	440	60
$5 < p_T < 6$	$1.5 < y^* < 2.0$	$10\,090 \pm 910$	460	770	150
$5 < p_T < 6$	$2.0 < y^* < 2.5$	$9\,270 \pm 630$	270	560	80
$5 < p_T < 6$	$2.5 < y^* < 3.0$	$7\,560 \pm 500$	220	440	60
$5 < p_T < 6$	$3.0 < y^* < 3.5$	$6\,080 \pm 440$	210	380	50
$5 < p_T < 6$	$3.5 < y^* < 4.0$	$3\,710 \pm 350$	210	280	40
$6 < p_T < 7$	$1.5 < y^* < 2.0$	$6\,560 \pm 630$	330	520	120
$6 < p_T < 7$	$2.0 < y^* < 2.5$	$5\,600 \pm 430$	190	380	60
$6 < p_T < 7$	$2.5 < y^* < 3.0$	$4\,630 \pm 360$	160	320	50
$6 < p_T < 7$	$3.0 < y^* < 3.5$	$3\,620 \pm 290$	160	250	40
$6 < p_T < 7$	$3.5 < y^* < 4.0$	$2\,114 \pm 240$	161	176	32

Table 5

J/ψ-from-b-hadrons absolute production cross-section in pPb, as a function of p_T and y^*. The quoted uncertainties are the total uncertainties, and the breakdown into statistical uncertainties, and correlated and uncorrelated systematic uncertainties.

p_T bin (GeV/c)	y^* bin	$\frac{d^2\sigma}{dp_T dy^*}$ [nb/(GeV/c)]	stat.	corr.	uncorr.
$7 < p_T < 8$	$1.5 < y^* < 2.0$	$4\,610 \pm 430$	250	330	100
$7 < p_T < 8$	$2.0 < y^* < 2.5$	$3\,650 \pm 260$	140	210	50
$7 < p_T < 8$	$2.5 < y^* < 3.0$	$3\,010 \pm 230$	130	180	40
$7 < p_T < 8$	$3.0 < y^* < 3.5$	$2\,327 \pm 203$	123	157	34
$7 < p_T < 8$	$3.5 < y^* < 4.0$	$1\,432 \pm 183$	120	135	28
$8 < p_T < 9$	$1.5 < y^* < 2.0$	$2\,590 \pm 260$	180	170	70
$8 < p_T < 9$	$2.0 < y^* < 2.5$	$2\,300 \pm 180$	110	130	40
$8 < p_T < 9$	$2.5 < y^* < 3.0$	$1\,859 \pm 152$	99	110	31
$8 < p_T < 9$	$3.0 < y^* < 3.5$	$1\,273 \pm 126$	89	85	24
$8 < p_T < 9$	$3.5 < y^* < 4.0$	$1\,002 \pm 139$	92	100	26
$9 < p_T < 10$	$1.5 < y^* < 2.0$	$1\,770 \pm 190$	140	120	60
$9 < p_T < 10$	$2.0 < y^* < 2.5$	$1\,529 \pm 127$	87	87	30
$9 < p_T < 10$	$2.5 < y^* < 3.0$	$1\,142 \pm 107$	75	72	23
$9 < p_T < 10$	$3.0 < y^* < 3.5$	864 ± 95	69	61	21
$9 < p_T < 10$	$3.5 < y^* < 4.0$	544 ± 90	67	57	17
$10 < p_T < 11$	$1.5 < y^* < 2.0$	$1\,070 \pm 130$	100	60	40
$10 < p_T < 11$	$2.0 < y^* < 2.5$	917 ± 88	66	52	22
$10 < p_T < 11$	$2.5 < y^* < 3.0$	804 ± 83	64	47	21
$10 < p_T < 11$	$3.0 < y^* < 3.5$	477 ± 63	51	35	14
$10 < p_T < 11$	$3.5 < y^* < 4.0$	397 ± 73	51	50	15
$11 < p_T < 12$	$1.5 < y^* < 2.0$	800 ± 100	80	50	40
$11 < p_T < 12$	$2.0 < y^* < 2.5$	678 ± 72	57	38	21
$11 < p_T < 12$	$2.5 < y^* < 3.0$	446 ± 60	50	27	15

Table 5 (_Continued_)

p_T bin (GeV/c)	y^* bin	$\frac{d^2\sigma}{dp_T dy^*}$ [nb/(GeV/c)]	stat.	corr.	uncorr.
$11 < p_T < 12$	$3.0 < y^* < 3.5$	386 ± 57	47	29	14
$11 < p_T < 12$	$3.5 < y^* < 4.0$	162 ± 41	37	15	8
$12 < p_T < 13$	$1.5 < y^* < 2.0$	526 ± 80	65	33	32
$12 < p_T < 13$	$2.0 < y^* < 2.5$	474 ± 57	45	29	16
$12 < p_T < 13$	$2.5 < y^* < 3.0$	370 ± 48	39	23	15
$12 < p_T < 13$	$3.0 < y^* < 3.5$	231 ± 40	34	18	11
$12 < p_T < 13$	$3.5 < y^* < 4.0$	153 ± 37	29	21	7
$13 < p_T < 14$	$1.5 < y^* < 2.0$	419 ± 67	56	24	28
$13 < p_T < 14$	$2.0 < y^* < 2.5$	387 ± 48	39	22	16
$13 < p_T < 14$	$2.5 < y^* < 3.0$	224 ± 35	31	13	11
$13 < p_T < 14$	$3.0 < y^* < 3.5$	151 ± 27	23	11	6
$13 < p_T < 14$	$3.5 < y^* < 4.0$	100 ± 27	24	9	7

A.3. $\frac{d^2\sigma}{dp_T dy^*}$ for prompt J/ψ in Pbp

Table 6
Prompt J/ψ absolute production cross-section in Pbp, as a function of p_T and y^*. The quoted uncertainties are the total uncertainties, and the breakdown into statistical uncertainties, and correlated and uncorrelated systematic uncertainties.

p_T bin (GeV/c)	y^* bin	$\frac{d^2\sigma}{dp_T dy^*}$ [nb/(GeV/c)]	stat.	corr.	uncorr.
$0 < p_T < 1$	$-3.0 < y^* < -2.5$	$132\,900 \pm 23\,100$	2300	22800	2500
$0 < p_T < 1$	$-3.5 < y^* < -3.0$	$114\,000 \pm 13\,100$	1300	13000	1200
$0 < p_T < 1$	$-4.0 < y^* < -3.5$	$96\,600 \pm 9300$	1200	9200	900
$0 < p_T < 1$	$-4.5 < y^* < -4.0$	$83\,600 \pm 6900$	1200	6800	800
$0 < p_T < 1$	$-5.0 < y^* < -4.5$	$70\,500 \pm 6600$	1400	6300	1000
$1 < p_T < 2$	$-3.0 < y^* < -2.5$	$263\,000 \pm 34\,800$	2900	34600	2800
$1 < p_T < 2$	$-3.5 < y^* < -3.0$	$226\,900 \pm 21\,600$	1800	21500	1400
$1 < p_T < 2$	$-4.0 < y^* < -3.5$	$188\,300 \pm 15\,900$	1500	15800	1100
$1 < p_T < 2$	$-4.5 < y^* < -4.0$	$161\,400 \pm 12\,500$	1500	12300	1000
$1 < p_T < 2$	$-5.0 < y^* < -4.5$	$135\,700 \pm 16\,300$	1800	16100	1200
$2 < p_T < 3$	$-3.0 < y^* < -2.5$	$230\,900 \pm 27\,400$	2400	27200	2400
$2 < p_T < 3$	$-3.5 < y^* < -3.0$	$198\,600 \pm 18\,400$	1600	18300	1300
$2 < p_T < 3$	$-4.0 < y^* < -3.5$	$167\,000 \pm 13\,000$	1000	13000	1000
$2 < p_T < 3$	$-4.5 < y^* < -4.0$	$128\,700 \pm 10\,600$	1300	10400	900
$2 < p_T < 3$	$-5.0 < y^* < -4.5$	$98\,400 \pm 14\,700$	1500	14600	1000
$3 < p_T < 4$	$-3.0 < y^* < -2.5$	$144\,600 \pm 18\,400$	1700	18300	1700
$3 < p_T < 4$	$-3.5 < y^* < -3.0$	$128\,400 \pm 13\,000$	1100	12900	900
$3 < p_T < 4$	$-4.0 < y^* < -3.5$	$104\,600 \pm 9300$	900	9200	700
$3 < p_T < 4$	$-4.5 < y^* < -4.0$	$77\,600 \pm 8100$	900	8000	600
$3 < p_T < 4$	$-5.0 < y^* < -4.5$	$55\,300 \pm 9400$	1000	9300	700
$4 < p_T < 5$	$-3.0 < y^* < -2.5$	$83\,600 \pm 9600$	1100	9500	1200
$4 < p_T < 5$	$-3.5 < y^* < -3.0$	$71\,400 \pm 6600$	700	6500	600
$4 < p_T < 5$	$-4.0 < y^* < -3.5$	$55\,900 \pm 4600$	600	4600	500
$4 < p_T < 5$	$-4.5 < y^* < -4.0$	$40\,500 \pm 4900$	500	4800	400
$4 < p_T < 5$	$-5.0 < y^* < -4.5$	$25\,600 \pm 4600$	600	4600	400
$5 < p_T < 6$	$-3.0 < y^* < -2.5$	$46\,600 \pm 5000$	700	4900	800
$5 < p_T < 6$	$-3.5 < y^* < -3.0$	$37\,100 \pm 3300$	400	3300	400
$5 < p_T < 6$	$-4.0 < y^* < -3.5$	$27\,810 \pm 2400$	350	2350	330
$5 < p_T < 6$	$-4.5 < y^* < -4.0$	$19\,990 \pm 2770$	320	2730	290
$5 < p_T < 6$	$-5.0 < y^* < -4.5$	$13\,540 \pm 2660$	380	2620	320
$6 < p_T < 7$	$-3.0 < y^* < -2.5$	$22\,500 \pm 2500$	400	2400	500
$6 < p_T < 7$	$-3.5 < y^* < -3.0$	$19\,950 \pm 1830$	290	1780	320
$6 < p_T < 7$	$-4.0 < y^* < -3.5$	$14\,620 \pm 1440$	240	1400	260
$6 < p_T < 7$	$-4.5 < y^* < -4.0$	$10\,330 \pm 1630$	220	1600	230
$6 < p_T < 7$	$-5.0 < y^* < -4.5$	5670 ± 1260	240	1220	200

Table 7
Prompt J/ψ absolute production cross-section in Pbp, as a function of p_T and y^*. The quoted uncertainties are the total uncertainties, and the breakdown into statistical uncertainties, and correlated and uncorrelated systematic uncertainties.

p_T bin (GeV/c)	y^* bin	$\frac{d^2\sigma}{dp_T dy^*}$ [nb/(GeV/c)]	stat.	corr.	uncorr.
$7 < p_T < 8$	$-3.0 < y^* < -2.5$	$12\,260 \pm 1220$	290	1130	350
$7 < p_T < 8$	$-3.5 < y^* < -3.0$	$10\,320 \pm 970$	190	920	220
$7 < p_T < 8$	$-4.0 < y^* < -3.5$	7480 ± 790	170	760	180
$7 < p_T < 8$	$-4.5 < y^* < -4.0$	4760 ± 820	140	800	150
$7 < p_T < 8$	$-5.0 < y^* < -4.5$	2930 ± 730	160	700	140

Table 7 (_Continued_)

p_T bin (GeV/c)	y^* bin	$\frac{d^2\sigma}{dp_T dy^*}$ [nb/(GeV/c)]	stat.	corr.	uncorr.
$8 < p_T < 9$	$-3.0 < y^* < -2.5$	6690 ± 700	210	610	270
$8 < p_T < 9$	$-3.5 < y^* < -3.0$	5850 ± 560	150	500	180
$8 < p_T < 9$	$-4.0 < y^* < -3.5$	3970 ± 510	120	480	130
$8 < p_T < 9$	$-4.5 < y^* < -4.0$	2320 ± 440	90	420	100
$8 < p_T < 9$	$-5.0 < y^* < -4.5$	1110 ± 310	100	290	60
$9 < p_T < 10$	$-3.0 < y^* < -2.5$	4050 ± 450	150	370	210
$9 < p_T < 10$	$-3.5 < y^* < -3.0$	3000 ± 300	100	300	100
$9 < p_T < 10$	$-4.0 < y^* < -3.5$	1940 ± 290	80	260	80
$9 < p_T < 10$	$-4.5 < y^* < -4.0$	1290 ± 270	70	250	80
$9 < p_T < 10$	$-5.0 < y^* < -4.5$	670 ± 200	70	170	70
$10 < p_T < 11$	$-3.0 < y^* < -2.5$	2230 ± 240	100	180	130
$10 < p_T < 11$	$-3.5 < y^* < -3.0$	1890 ± 210	80	160	100
$10 < p_T < 11$	$-4.0 < y^* < -3.5$	1180 ± 190	60	160	70
$10 < p_T < 11$	$-4.5 < y^* < -4.0$	590 ± 130	40	120	40
$10 < p_T < 11$	$-5.0 < y^* < -4.5$	297 ± 99	42	82	35
$11 < p_T < 12$	$-3.0 < y^* < -2.5$	1300 ± 160	80	100	100
$11 < p_T < 12$	$-3.5 < y^* < -3.0$	930 ± 110	50	90	50
$11 < p_T < 12$	$-4.0 < y^* < -3.5$	600 ± 110	50	80	50
$11 < p_T < 12$	$-4.5 < y^* < -4.0$	420 ± 110	40	90	40
$11 < p_T < 12$	$-5.0 < y^* < -4.5$	210 ± 80	40	50	40
$12 < p_T < 13$	$-3.0 < y^* < -2.5$	980 ± 140	70	90	90
$12 < p_T < 13$	$-3.5 < y^* < -3.0$	660 ± 100	50	60	60
$12 < p_T < 13$	$-4.0 < y^* < -3.5$	313 ± 64	32	46	29
$12 < p_T < 13$	$-4.5 < y^* < -4.0$	229 ± 67	27	50	34
$12 < p_T < 13$	$-5.0 < y^* < -4.5$	140 ± 70	40	40	50
$13 < p_T < 14$	$-3.0 < y^* < -2.5$	550 ± 100	60	40	60
$13 < p_T < 14$	$-3.5 < y^* < -3.0$	328 ± 60	40	32	30
$13 < p_T < 14$	$-4.0 < y^* < -3.5$	248 ± 64	27	37	43
$13 < p_T < 14$	$-4.5 < y^* < -4.0$	135 ± 54	23	32	36
$13 < p_T < 14$	$-5.0 < y^* < -4.5$	29 ± 14	10	7	6

A.4. $\frac{d^2\sigma}{dp_T dy^*}$ for J/ψ-from-b-hadrons in Pbp

Table 8
J/ψ-from-b-hadrons absolute production cross-section in Pbp, as a function of p_T and y^*. The quoted uncertainties are the total uncertainties, and the breakdown into statistical uncertainties, and correlated and uncorrelated systematic uncertainties.

p_T bin (GeV/c)	y^* bin	$\frac{d^2\sigma}{dp_T dy^*}$ [nb/(GeV/c)]	stat.	corr.	uncorr.
$0 < p_T < 1$	$-3.0 < y^* < -2.5$	$16\,120 \pm 2890$	770	2770	300
$0 < p_T < 1$	$-3.5 < y^* < -3.0$	$11\,760 \pm 1400$	400	1340	120
$0 < p_T < 1$	$-4.0 < y^* < -3.5$	9270 ± 950	330	880	80
$0 < p_T < 1$	$-4.5 < y^* < -4.0$	7000 ± 650	320	570	70
$0 < p_T < 1$	$-5.0 < y^* < -4.5$	4750 ± 580	390	430	70
$1 < p_T < 2$	$-3.0 < y^* < -2.5$	$35\,000 \pm 4700$	1000	4600	400
$1 < p_T < 2$	$-3.5 < y^* < -3.0$	$26\,050 \pm 2540$	560	2470	170
$1 < p_T < 2$	$-4.0 < y^* < -3.5$	$20\,280 \pm 1770$	450	1710	120
$1 < p_T < 2$	$-4.5 < y^* < -4.0$	$14\,270 \pm 1170$	420	1090	90
$1 < p_T < 2$	$-5.0 < y^* < -4.5$	9630 ± 1250	490	1140	90
$2 < p_T < 3$	$-3.0 < y^* < -2.5$	$31\,420 \pm 3810$	850	3700	320
$2 < p_T < 3$	$-3.5 < y^* < -3.0$	$25\,560 \pm 2410$	510	2350	160
$2 < p_T < 3$	$-4.0 < y^* < -3.5$	$19\,830 \pm 1640$	420	1580	110
$2 < p_T < 3$	$-4.5 < y^* < -4.0$	$12\,690 \pm 1100$	370	1030	80
$2 < p_T < 3$	$-5.0 < y^* < -4.5$	7760 ± 1230	400	1150	80
$3 < p_T < 4$	$-3.0 < y^* < -2.5$	$21\,880 \pm 2840$	630	2760	250
$3 < p_T < 4$	$-3.5 < y^* < -3.0$	$19\,200 \pm 1980$	390	1940	140
$3 < p_T < 4$	$-4.0 < y^* < -3.5$	$13\,490 \pm 1230$	310	1190	90
$3 < p_T < 4$	$-4.5 < y^* < -4.0$	8720 ± 940	270	900	70
$3 < p_T < 4$	$-5.0 < y^* < -4.5$	4420 ± 800	280	750	60
$4 < p_T < 5$	$-3.0 < y^* < -2.5$	$14\,340 \pm 1700$	440	1630	200
$4 < p_T < 5$	$-3.5 < y^* < -3.0$	$11\,200 \pm 1060$	260	1020	100
$4 < p_T < 5$	$-4.0 < y^* < -3.5$	8210 ± 710	220	670	70
$4 < p_T < 5$	$-4.5 < y^* < -4.0$	4920 ± 620	180	590	50
$4 < p_T < 5$	$-5.0 < y^* < -4.5$	2660 ± 520	190	480	50
$5 < p_T < 6$	$-3.0 < y^* < -2.5$	7640 ± 870	290	800	140
$5 < p_T < 6$	$-3.5 < y^* < -3.0$	6730 ± 630	180	590	80
$5 < p_T < 6$	$-4.0 < y^* < -3.5$	4370 ± 400	140	370	50
$5 < p_T < 6$	$-4.5 < y^* < -4.0$	2740 ± 400	120	380	40
$5 < p_T < 6$	$-5.0 < y^* < -4.5$	1550 ± 330	130	300	40
$6 < p_T < 7$	$-3.0 < y^* < -2.5$	4400 ± 500	200	500	100
$6 < p_T < 7$	$-3.5 < y^* < -3.0$	3920 ± 380	130	350	60

Table 8 (*Continued*)

p_T bin (GeV/c)	y^* bin	$\frac{d^2\sigma}{dp_T dy^*}$ [nb/(GeV/c)]	stat.	corr.	uncorr.
$6 < p_T < 7$	$-4.0 < y^* < -3.5$	$2\,650 \pm 280$	110	250	50
$6 < p_T < 7$	$-4.5 < y^* < -4.0$	$1\,640 \pm 270$	90	250	40
$6 < p_T < 7$	$-5.0 < y^* < -4.5$	668 ± 170	89	143	23

Table 9

J/ψ-from-b-hadrons absolute production cross-section in Pbp, as a function of p_T and y^*. The quoted uncertainties are the total uncertainties, and the breakdown into statistical uncertainties, and correlated and uncorrelated systematic uncertainties.

p_T bin (GeV/c)	y^* bin	$\frac{d^2\sigma}{dp_T dy^*}$ [nb/(GeV/c)]	stat.	corr.	uncorr.
$7 < p_T < 8$	$-3.0 < y^* < -2.5$	$2\,860 \pm 310$	150	260	80
$7 < p_T < 8$	$-3.5 < y^* < -3.0$	$2\,340 \pm 230$	90	210	50
$7 < p_T < 8$	$-4.0 < y^* < -3.5$	$1\,414 \pm 165$	77	142	34
$7 < p_T < 8$	$-4.5 < y^* < -4.0$	748 ± 140	58	125	22
$7 < p_T < 8$	$-5.0 < y^* < -4.5$	374 ± 105	52	89	17
$8 < p_T < 9$	$-3.0 < y^* < -2.5$	$2\,090 \pm 240$	120	190	80
$8 < p_T < 9$	$-3.5 < y^* < -3.0$	$1\,450 \pm 150$	70	120	40
$8 < p_T < 9$	$-4.0 < y^* < -3.5$	812 ± 114	54	97	25
$8 < p_T < 9$	$-4.5 < y^* < -4.0$	474 ± 99	44	86	19
$8 < p_T < 9$	$-5.0 < y^* < -4.5$	207 ± 66	36	53	12
$9 < p_T < 10$	$-3.0 < y^* < -2.5$	$1\,370 \pm 170$	90	120	70
$9 < p_T < 10$	$-3.5 < y^* < -3.0$	794 ± 97	53	76	29
$9 < p_T < 10$	$-4.0 < y^* < -3.5$	488 ± 80	40	66	21
$9 < p_T < 10$	$-4.5 < y^* < -4.0$	266 ± 63	33	51	16
$9 < p_T < 10$	$-5.0 < y^* < -4.5$	94 ± 37	26	23	9
$10 < p_T < 11$	$-3.0 < y^* < -2.5$	700 ± 90	60	60	40
$10 < p_T < 11$	$-3.5 < y^* < -3.0$	479 ± 65	44	41	24
$10 < p_T < 11$	$-4.0 < y^* < -3.5$	372 ± 65	35	50	22
$10 < p_T < 11$	$-4.5 < y^* < -4.0$	152 ± 39	22	30	9
$10 < p_T < 11$	$-5.0 < y^* < -4.5$	42 ± 19	14	11	5
$11 < p_T < 12$	$-3.0 < y^* < -2.5$	670 ± 90	60	50	50
$11 < p_T < 12$	$-3.5 < y^* < -3.0$	373 ± 53	35	34	21
$11 < p_T < 12$	$-4.0 < y^* < -3.5$	191 ± 40	26	25	15
$11 < p_T < 12$	$-4.5 < y^* < -4.0$	57 ± 20	14	12	5
$11 < p_T < 12$	$-5.0 < y^* < -4.5$	88 ± 36	22	23	17
$12 < p_T < 13$	$-3.0 < y^* < -2.5$	440 ± 70	40	40	40
$12 < p_T < 13$	$-3.5 < y^* < -3.0$	247 ± 43	29	22	23
$12 < p_T < 13$	$-4.0 < y^* < -3.5$	107 ± 27	20	15	10
$12 < p_T < 13$	$-4.5 < y^* < -4.0$	70 ± 24	16	15	10
$12 < p_T < 13$	$-5.0 < y^* < -4.5$	19 ± 15	12	5	7
$13 < p_T < 14$	$-3.0 < y^* < -2.5$	257 ± 53	39	19	30
$13 < p_T < 14$	$-3.5 < y^* < -3.0$	146 ± 33	27	14	13
$13 < p_T < 14$	$-4.0 < y^* < -3.5$	114 ± 32	19	17	20
$13 < p_T < 14$	$-4.5 < y^* < -4.0$	40 ± 19	12	9	10
$13 < p_T < 14$	$-5.0 < y^* < -4.5$	10 ± 7	6	2	2

A.5. Fraction of J/ψ-from-b-hadrons in pPb

Table 10

Fraction of J/ψ-from-b-hadrons, f_b, in pPb in bins of p_T and y^*. The uncertainty is the quadratic sum of statistical and systematic uncertainties.

p_T bin (GeV/c)	y^* bin	f_b
$0 < p_T < 1$	$1.5 < y^* < 2.0$	0.13 ± 0.01
$0 < p_T < 1$	$2.0 < y^* < 2.5$	0.12 ± 0.01
$0 < p_T < 1$	$2.5 < y^* < 3.0$	0.11 ± 0.01
$0 < p_T < 1$	$3.0 < y^* < 3.5$	0.11 ± 0.01
$0 < p_T < 1$	$3.5 < y^* < 4.0$	0.10 ± 0.01
$1 < p_T < 2$	$1.5 < y^* < 2.0$	0.13 ± 0.01
$1 < p_T < 2$	$2.0 < y^* < 2.5$	0.13 ± 0.01
$1 < p_T < 2$	$2.5 < y^* < 3.0$	0.13 ± 0.01
$1 < p_T < 2$	$3.0 < y^* < 3.5$	0.12 ± 0.01
$1 < p_T < 2$	$3.5 < y^* < 4.0$	0.12 ± 0.01
$2 < p_T < 3$	$1.5 < y^* < 2.0$	0.15 ± 0.01
$2 < p_T < 3$	$2.0 < y^* < 2.5$	0.15 ± 0.01
$2 < p_T < 3$	$2.5 < y^* < 3.0$	0.14 ± 0.01
$2 < p_T < 3$	$3.0 < y^* < 3.5$	0.14 ± 0.01
$2 < p_T < 3$	$3.5 < y^* < 4.0$	0.12 ± 0.01
$3 < p_T < 4$	$1.5 < y^* < 2.0$	0.15 ± 0.01

Table 10 (*Continued*)

p_T bin (GeV/c)	y^* bin	f_b
$3 < p_T < 4$	$2.0 < y^* < 2.5$	0.16 ± 0.01
$3 < p_T < 4$	$2.5 < y^* < 3.0$	0.15 ± 0.01
$3 < p_T < 4$	$3.0 < y^* < 3.5$	0.14 ± 0.01
$3 < p_T < 4$	$3.5 < y^* < 4.0$	0.13 ± 0.01
$4 < p_T < 5$	$1.5 < y^* < 2.0$	0.16 ± 0.01
$4 < p_T < 5$	$2.0 < y^* < 2.5$	0.17 ± 0.01
$4 < p_T < 5$	$2.5 < y^* < 3.0$	0.16 ± 0.01
$4 < p_T < 5$	$3.0 < y^* < 3.5$	0.15 ± 0.01
$4 < p_T < 5$	$3.5 < y^* < 4.0$	0.14 ± 0.01
$5 < p_T < 6$	$1.5 < y^* < 2.0$	0.18 ± 0.01
$5 < p_T < 6$	$2.0 < y^* < 2.5$	0.18 ± 0.01
$5 < p_T < 6$	$2.5 < y^* < 3.0$	0.18 ± 0.01
$5 < p_T < 6$	$3.0 < y^* < 3.5$	0.17 ± 0.01
$5 < p_T < 6$	$3.5 < y^* < 4.0$	0.15 ± 0.01
$6 < p_T < 7$	$1.5 < y^* < 2.0$	0.21 ± 0.01
$6 < p_T < 7$	$2.0 < y^* < 2.5$	0.19 ± 0.01
$6 < p_T < 7$	$2.5 < y^* < 3.0$	0.20 ± 0.01
$6 < p_T < 7$	$3.0 < y^* < 3.5$	0.19 ± 0.01
$6 < p_T < 7$	$3.5 < y^* < 4.0$	0.15 ± 0.01

Table 11

Fraction of J/ψ-from-b-hadrons, f_b, in pPb in bins of p_T and y^*. The uncertainty is the quadratic sum of statistical and systematic uncertainties.

p_T bin (GeV/c)	y^* bin	f_b
$7 < p_T < 8$	$1.5 < y^* < 2.0$	0.24 ± 0.01
$7 < p_T < 8$	$2.0 < y^* < 2.5$	0.22 ± 0.01
$7 < p_T < 8$	$2.5 < y^* < 3.0$	0.23 ± 0.01
$7 < p_T < 8$	$3.0 < y^* < 3.5$	0.21 ± 0.01
$7 < p_T < 8$	$3.5 < y^* < 4.0$	0.19 ± 0.01
$8 < p_T < 9$	$1.5 < y^* < 2.0$	0.25 ± 0.02
$8 < p_T < 9$	$2.0 < y^* < 2.5$	0.24 ± 0.01
$8 < p_T < 9$	$2.5 < y^* < 3.0$	0.23 ± 0.01
$8 < p_T < 9$	$3.0 < y^* < 3.5$	0.22 ± 0.01
$8 < p_T < 9$	$3.5 < y^* < 4.0$	0.21 ± 0.02
$9 < p_T < 10$	$1.5 < y^* < 2.0$	0.27 ± 0.02
$9 < p_T < 10$	$2.0 < y^* < 2.5$	0.26 ± 0.01
$9 < p_T < 10$	$2.5 < y^* < 3.0$	0.25 ± 0.01
$9 < p_T < 10$	$3.0 < y^* < 3.5$	0.24 ± 0.02
$9 < p_T < 10$	$3.5 < y^* < 4.0$	0.20 ± 0.02
$10 < p_T < 11$	$1.5 < y^* < 2.0$	0.29 ± 0.02
$10 < p_T < 11$	$2.0 < y^* < 2.5$	0.26 ± 0.02
$10 < p_T < 11$	$2.5 < y^* < 3.0$	0.26 ± 0.02
$10 < p_T < 11$	$3.0 < y^* < 3.5$	0.24 ± 0.02
$10 < p_T < 11$	$3.5 < y^* < 4.0$	0.26 ± 0.03
$11 < p_T < 12$	$1.5 < y^* < 2.0$	0.30 ± 0.03
$11 < p_T < 12$	$2.0 < y^* < 2.5$	0.30 ± 0.02
$11 < p_T < 12$	$2.5 < y^* < 3.0$	0.25 ± 0.03
$11 < p_T < 12$	$3.0 < y^* < 3.5$	0.28 ± 0.03
$11 < p_T < 12$	$3.5 < y^* < 4.0$	0.18 ± 0.04
$12 < p_T < 13$	$1.5 < y^* < 2.0$	0.31 ± 0.03
$12 < p_T < 13$	$2.0 < y^* < 2.5$	0.33 ± 0.03
$12 < p_T < 13$	$2.5 < y^* < 3.0$	0.32 ± 0.03
$12 < p_T < 13$	$3.0 < y^* < 3.5$	0.30 ± 0.04
$12 < p_T < 13$	$3.5 < y^* < 4.0$	0.26 ± 0.04
$13 < p_T < 14$	$1.5 < y^* < 2.0$	0.36 ± 0.04
$13 < p_T < 14$	$2.0 < y^* < 2.5$	0.39 ± 0.03
$13 < p_T < 14$	$2.5 < y^* < 3.0$	0.32 ± 0.04
$13 < p_T < 14$	$3.0 < y^* < 3.5$	0.30 ± 0.04
$13 < p_T < 14$	$3.5 < y^* < 4.0$	0.29 ± 0.06

A.6. Fraction of J/ψ-from-b-hadrons in Pbp

Table 12

Fraction of J/ψ-from-b-hadrons, f_b, in Pbp in bins of p_T and y^*. The uncertainty is the quadratic sum of statistical and systematic uncertainties.

p_T bin (GeV/c)	y^* bin	f_b
$0 < p_T < 1$	$-3.0 < y^* < -2.5$	0.11 ± 0.01
$0 < p_T < 1$	$-3.5 < y^* < -3.0$	0.09 ± 0.01
$0 < p_T < 1$	$-4.0 < y^* < -3.5$	0.09 ± 0.01
$0 < p_T < 1$	$-4.5 < y^* < -4.0$	0.08 ± 0.01
$0 < p_T < 1$	$-5.0 < y^* < -4.5$	0.06 ± 0.01

Table 12 (*Continued*)

p_T bin (GeV/c)	y^* bin	f_b
$1 < p_T < 2$	$-3.0 < y^* < -2.5$	0.12 ± 0.01
$1 < p_T < 2$	$-3.5 < y^* < -3.0$	0.10 ± 0.01
$1 < p_T < 2$	$-4.0 < y^* < -3.5$	0.10 ± 0.01
$1 < p_T < 2$	$-4.5 < y^* < -4.0$	0.08 ± 0.01
$1 < p_T < 2$	$-5.0 < y^* < -4.5$	0.07 ± 0.01
$2 < p_T < 3$	$-3.0 < y^* < -2.5$	0.12 ± 0.01
$2 < p_T < 3$	$-3.5 < y^* < -3.0$	0.11 ± 0.01
$2 < p_T < 3$	$-4.0 < y^* < -3.5$	0.11 ± 0.01
$2 < p_T < 3$	$-4.5 < y^* < -4.0$	0.09 ± 0.01
$2 < p_T < 3$	$-5.0 < y^* < -4.5$	0.07 ± 0.01
$3 < p_T < 4$	$-3.0 < y^* < -2.5$	0.13 ± 0.01
$3 < p_T < 4$	$-3.5 < y^* < -3.0$	0.13 ± 0.01
$3 < p_T < 4$	$-4.0 < y^* < -3.5$	0.11 ± 0.01
$3 < p_T < 4$	$-4.5 < y^* < -4.0$	0.10 ± 0.01
$3 < p_T < 4$	$-5.0 < y^* < -4.5$	0.07 ± 0.01
$4 < p_T < 5$	$-3.0 < y^* < -2.5$	0.15 ± 0.01
$4 < p_T < 5$	$-3.5 < y^* < -3.0$	0.14 ± 0.01
$4 < p_T < 5$	$-4.0 < y^* < -3.5$	0.13 ± 0.01
$4 < p_T < 5$	$-4.5 < y^* < -4.0$	0.11 ± 0.01
$4 < p_T < 5$	$-5.0 < y^* < -4.5$	0.09 ± 0.01
$5 < p_T < 6$	$-3.0 < y^* < -2.5$	0.14 ± 0.01
$5 < p_T < 6$	$-3.5 < y^* < -3.0$	0.15 ± 0.01
$5 < p_T < 6$	$-4.0 < y^* < -3.5$	0.14 ± 0.01
$5 < p_T < 6$	$-4.5 < y^* < -4.0$	0.12 ± 0.01
$5 < p_T < 6$	$-5.0 < y^* < -4.5$	0.10 ± 0.01
$6 < p_T < 7$	$-3.0 < y^* < -2.5$	0.16 ± 0.01
$6 < p_T < 7$	$-3.5 < y^* < -3.0$	0.16 ± 0.01
$6 < p_T < 7$	$-4.0 < y^* < -3.5$	0.15 ± 0.01
$6 < p_T < 7$	$-4.5 < y^* < -4.0$	0.14 ± 0.01
$6 < p_T < 7$	$-5.0 < y^* < -4.5$	0.11 ± 0.01

Table 13

Fraction of J/ψ-from-b-hadrons, f_b, in Pbp in bins of p_T and y^*. The uncertainty is the quadratic sum of statistical and systematic uncertainties.

p_T bin (GeV/c)	y^* bin	f_b
$7 < p_T < 8$	$-3.0 < y^* < -2.5$	0.19 ± 0.01
$7 < p_T < 8$	$-3.5 < y^* < -3.0$	0.18 ± 0.01
$7 < p_T < 8$	$-4.0 < y^* < -3.5$	0.16 ± 0.01
$7 < p_T < 8$	$-4.5 < y^* < -4.0$	0.14 ± 0.01
$7 < p_T < 8$	$-5.0 < y^* < -4.5$	0.11 ± 0.02
$8 < p_T < 9$	$-3.0 < y^* < -2.5$	0.24 ± 0.01
$8 < p_T < 9$	$-3.5 < y^* < -3.0$	0.20 ± 0.01
$8 < p_T < 9$	$-4.0 < y^* < -3.5$	0.17 ± 0.01
$8 < p_T < 9$	$-4.5 < y^* < -4.0$	0.17 ± 0.01
$8 < p_T < 9$	$-5.0 < y^* < -4.5$	0.16 ± 0.03
$9 < p_T < 10$	$-3.0 < y^* < -2.5$	0.25 ± 0.01
$9 < p_T < 10$	$-3.5 < y^* < -3.0$	0.21 ± 0.01
$9 < p_T < 10$	$-4.0 < y^* < -3.5$	0.20 ± 0.02
$9 < p_T < 10$	$-4.5 < y^* < -4.0$	0.17 ± 0.02
$9 < p_T < 10$	$-5.0 < y^* < -4.5$	0.12 ± 0.03
$10 < p_T < 11$	$-3.0 < y^* < -2.5$	0.24 ± 0.02
$10 < p_T < 11$	$-3.5 < y^* < -3.0$	0.20 ± 0.02
$10 < p_T < 11$	$-4.0 < y^* < -3.5$	0.24 ± 0.02
$10 < p_T < 11$	$-4.5 < y^* < -4.0$	0.21 ± 0.03
$10 < p_T < 11$	$-5.0 < y^* < -4.5$	0.13 ± 0.04
$11 < p_T < 12$	$-3.0 < y^* < -2.5$	0.34 ± 0.02
$11 < p_T < 12$	$-3.5 < y^* < -3.0$	0.29 ± 0.02
$11 < p_T < 12$	$-4.0 < y^* < -3.5$	0.24 ± 0.03
$11 < p_T < 12$	$-4.5 < y^* < -4.0$	0.12 ± 0.03
$11 < p_T < 12$	$-5.0 < y^* < -4.5$	0.30 ± 0.07
$12 < p_T < 13$	$-3.0 < y^* < -2.5$	0.31 ± 0.03
$12 < p_T < 13$	$-3.5 < y^* < -3.0$	0.27 ± 0.03
$12 < p_T < 13$	$-4.0 < y^* < -3.5$	0.25 ± 0.04
$12 < p_T < 13$	$-4.5 < y^* < -4.0$	0.24 ± 0.05
$12 < p_T < 13$	$-5.0 < y^* < -4.5$	0.12 ± 0.07
$13 < p_T < 14$	$-3.0 < y^* < -2.5$	0.32 ± 0.05
$13 < p_T < 14$	$-3.5 < y^* < -3.0$	0.31 ± 0.06
$13 < p_T < 14$	$-4.0 < y^* < -3.5$	0.32 ± 0.04
$13 < p_T < 14$	$-4.5 < y^* < -4.0$	0.23 ± 0.06
$13 < p_T < 14$	$-5.0 < y^* < -4.5$	0.27 ± 0.14

Appendix B. Nuclear modification factor numerical results

B.1. $R_{p\mathrm{Pb}}$ for prompt J/ψ

Table 14

Prompt J/ψ nuclear modification factor, $R_{p\mathrm{Pb}}$, in pPb and Pbp as a function of p_T integrated over y^* in the range $1.5 < y^* < 4.0$ for pPb and $-5.0 < y^* < -2.5$ for Pbp. The quoted uncertainties are the quadratic sums of statistical and systematic uncertainties.

p_T bin (GeV/c)	$R_{p\mathrm{Pb}}$ in pPb	$R_{p\mathrm{Pb}}$ in Pbp
$0 < p_T < 1$	0.53 ± 0.06	0.75 ± 0.10
$1 < p_T < 2$	0.56 ± 0.06	0.81 ± 0.10
$2 < p_T < 3$	0.65 ± 0.06	0.93 ± 0.12
$3 < p_T < 4$	0.72 ± 0.07	0.99 ± 0.14
$4 < p_T < 5$	0.76 ± 0.08	1.02 ± 0.15
$5 < p_T < 6$	0.81 ± 0.08	1.06 ± 0.16
$6 < p_T < 7$	0.86 ± 0.09	1.08 ± 0.18
$7 < p_T < 8$	0.87 ± 0.10	1.06 ± 0.18
$8 < p_T < 9$	0.88 ± 0.10	1.06 ± 0.19
$9 < p_T < 10$	0.92 ± 0.11	1.07 ± 0.15
$10 < p_T < 11$	0.89 ± 0.11	1.02 ± 0.14
$11 < p_T < 12$	1.00 ± 0.12	0.97 ± 0.14
$12 < p_T < 13$	0.92 ± 0.13	1.07 ± 0.17
$13 < p_T < 14$	0.83 ± 0.13	0.89 ± 0.15

Table 15

Prompt J/ψ nuclear modification factor, $R_{p\mathrm{Pb}}$, in pPb and Pbp as a function of y^* integrated over p_T in the range $0 < p_T < 14$ GeV/c. The quoted uncertainties are the quadratic sums of statistical and systematic uncertainties.

y^* bin	$R_{p\mathrm{Pb}}$
$-4.5 < y^* < -4.0$	0.86 ± 0.10
$-4.0 < y^* < -3.5$	0.84 ± 0.09
$-3.5 < y^* < -3.0$	0.87 ± 0.10
$-3.0 < y^* < -2.5$	0.90 ± 0.13
$1.5 < y^* < 2.0$	0.68 ± 0.09
$2.0 < y^* < 2.5$	0.71 ± 0.07
$2.5 < y^* < 3.0$	0.62 ± 0.06
$3.0 < y^* < 3.5$	0.59 ± 0.05
$3.5 < y^* < 4.0$	0.57 ± 0.05

B.2. $R_{p\mathrm{Pb}}$ for J/ψ-from-b-hadrons

Table 16

J/ψ-from-b-hadrons nuclear modification factor, $R_{p\mathrm{Pb}}$, in pPb and Pbp as a function of p_T integrated over y^* in the range $1.5 < y^* < 4.0$ for pPb and $-5.0 < y^* < -2.5$ for Pbp. The quoted uncertainties are the quadratic sums of statistical and systematic uncertainties.

p_T bin (GeV/c)	$R_{p\mathrm{Pb}}$ in pPb	$R_{p\mathrm{Pb}}$ in Pbp
$0 < p_T < 1$	0.75 ± 0.12	1.05 ± 0.19
$1 < p_T < 2$	0.79 ± 0.09	1.05 ± 0.16
$2 < p_T < 3$	0.82 ± 0.09	1.07 ± 0.17
$3 < p_T < 4$	0.85 ± 0.10	1.09 ± 0.18
$4 < p_T < 5$	0.87 ± 0.10	1.12 ± 0.20
$5 < p_T < 6$	0.91 ± 0.11	1.05 ± 0.13
$6 < p_T < 7$	0.91 ± 0.12	1.02 ± 0.14
$7 < p_T < 8$	0.99 ± 0.13	0.99 ± 0.13
$8 < p_T < 9$	0.94 ± 0.14	1.04 ± 0.14
$9 < p_T < 10$	0.94 ± 0.14	0.99 ± 0.15
$10 < p_T < 11$	0.91 ± 0.15	0.91 ± 0.14
$11 < p_T < 12$	0.87 ± 0.13	1.11 ± 0.18
$12 < p_T < 13$	0.89 ± 0.16	0.97 ± 0.18
$13 < p_T < 14$	0.96 ± 0.21	0.94 ± 0.19

Table 17

J/ψ-from-b-hadrons nuclear modification factor, $R_{p\mathrm{Pb}}$, in $p\mathrm{Pb}$ as a function of y^* integrated over p_T in the range $0 < p_\mathrm{T} < 14$ GeV/c. The quoted uncertainties are the quadratic sums of statistical and systematic uncertainties.

y^* bin	$R_{p\mathrm{Pb}}$
$-4.5 < y^* < -4.0$	1.10 ± 0.13
$-4.0 < y^* < -3.5$	1.03 ± 0.11
$-3.5 < y^* < -3.0$	0.97 ± 0.11
$-3.0 < y^* < -2.5$	1.00 ± 0.14
$1.5 < y^* < 2.0$	0.84 ± 0.17
$2.0 < y^* < 2.5$	0.89 ± 0.09
$2.5 < y^* < 3.0$	0.80 ± 0.07
$3.0 < y^* < 3.5$	0.80 ± 0.07
$3.5 < y^* < 4.0$	0.82 ± 0.08

Appendix C. Forward-to-backward ratios numerical results

C.1. R_{FB} for prompt J/ψ

Table 18

Prompt J/ψ forward-to-backward ratio, R_{FB}, as a function of p_T integrated over $|y^*|$ in the range $2.5 < |y^*| < 4.0$. The quoted uncertainties are the quadratic sums of statistical and systematic uncertainties.

p_T bin (GeV/c)	R_{FB}
$0 < p_\mathrm{T} < 1$	0.62 ± 0.07
$1 < p_\mathrm{T} < 2$	0.64 ± 0.06
$2 < p_\mathrm{T} < 3$	0.67 ± 0.06
$3 < p_\mathrm{T} < 4$	0.70 ± 0.06
$4 < p_\mathrm{T} < 5$	0.73 ± 0.07
$5 < p_\mathrm{T} < 6$	0.77 ± 0.07
$6 < p_\mathrm{T} < 7$	0.82 ± 0.07
$7 < p_\mathrm{T} < 8$	0.85 ± 0.08
$8 < p_\mathrm{T} < 9$	0.87 ± 0.09
$9 < p_\mathrm{T} < 10$	0.92 ± 0.10
$10 < p_\mathrm{T} < 11$	0.92 ± 0.10
$11 < p_\mathrm{T} < 12$	1.08 ± 0.13
$12 < p_\mathrm{T} < 13$	0.90 ± 0.12
$13 < p_\mathrm{T} < 14$	0.95 ± 0.15

Table 19

Prompt J/ψ forward-to-backward ratio, R_{FB}, as a function of y^* integrated over p_T in the range $0 < p_\mathrm{T} < 14$ GeV/c. The quoted uncertainties are the quadratic sums of statistical and systematic uncertainties.

y^* bin	R_{FB}
$2.5 < y^* < 3.0$	0.69 ± 0.08
$3.0 < y^* < 3.5$	0.67 ± 0.06
$3.5 < y^* < 4.0$	0.67 ± 0.05

C.2. R_{FB} for J/ψ-from-b-hadrons

Table 20

J/ψ-from-b-hadrons forward-to-backward ratio, R_{FB}, as a function of p_T integrated over $|y^*|$ in the range $2.5 < |y^*| < 4.0$. The quoted uncertainties are the quadratic sums of statistical and systematic uncertainties.

p_T bin (GeV/c)	R_{FB}
$0 < p_\mathrm{T} < 1$	0.72 ± 0.08
$1 < p_\mathrm{T} < 2$	0.76 ± 0.08
$2 < p_\mathrm{T} < 3$	0.79 ± 0.07
$3 < p_\mathrm{T} < 4$	0.80 ± 0.08

Table 20 (*Continued*)

p_T bin (GeV/c)	R_{FB}
$4 < p_\mathrm{T} < 5$	0.82 ± 0.08
$5 < p_\mathrm{T} < 6$	0.93 ± 0.09
$6 < p_\mathrm{T} < 7$	0.94 ± 0.09
$7 < p_\mathrm{T} < 8$	1.02 ± 0.10
$8 < p_\mathrm{T} < 9$	0.95 ± 0.10
$9 < p_\mathrm{T} < 10$	0.96 ± 0.11
$10 < p_\mathrm{T} < 11$	1.09 ± 0.14
$11 < p_\mathrm{T} < 12$	0.81 ± 0.12
$12 < p_\mathrm{T} < 13$	0.94 ± 0.15
$13 < p_\mathrm{T} < 14$	0.92 ± 0.17

Table 21

J/ψ-from-b-hadrons forward-to-backward ratio, R_{FB}, as a function of y^* integrated over p_T in the range $0 < p_\mathrm{T} < 14$ GeV/c. The quoted uncertainties are the quadratic sums of statistical and systematic uncertainties.

y^* bin	R_{FB}
$2.5 < y^* < 3.0$	0.80 ± 0.09
$3.0 < y^* < 3.5$	0.82 ± 0.07
$3.5 < y^* < 4.0$	0.79 ± 0.07

References

[1] T. Matsui, H. Satz, J/ψ suppression by quark–gluon plasma formation, Phys. Lett. B 178 (1986) 416.

[2] A. Mocsy, P. Petreczky, M. Strickland, Quarkonia in the quark–gluon plasma, Int. J. Mod. Phys. A 28 (2013) 1340012, arXiv:1302.2180.

[3] A. Andronic, et al., Heavy-flavour and quarkonium production in the LHC era: from proton–proton to heavy-ion collisions, Eur. Phys. J. C 76 (2016) 07, arXiv:1506.03981.

[4] ALICE collaboration, B. Abelev, et al., J/ψ suppression at forward rapidity in PbPb collisions at $\sqrt{s_{\mathrm{NN}}} = 2.76$ TeV, Phys. Rev. Lett. 109 (2012) 072301, arXiv:1202.1383.

[5] ALICE collaboration, B. Abelev, et al., Centrality, rapidity and transverse momentum dependence of J/ψ suppression in PbPb collisions at $\sqrt{s_{\mathrm{NN}}} = 2.76$ TeV, Phys. Lett. B 734 (2014) 314, arXiv:1311.0214.

[6] ALICE collaboration, J. Adam, et al., Inclusive, prompt and non-prompt J/ψ production at mid-rapidity in PbPb collisions at $\sqrt{s_{\mathrm{NN}}} = 2.76$ TeV, J. High Energy Phys. 07 (2015) 051, arXiv:1504.07151.

[7] ALICE collaboration, J. Adam, et al., Differential studies of inclusive J/ψ and $\psi(2S)$ production at forward rapidity in PbPb collisions at $\sqrt{s_{\mathrm{NN}}} = 2.76$ TeV, J. High Energy Phys. 05 (2016) 179, arXiv:1506.08804.

[8] ALICE collaboration, J. Adam, et al., J/ψ suppression at forward rapidity in PbPb collisions at $\sqrt{s_{\mathrm{NN}}} = 5.02$ TeV, Phys. Lett. B 766 (2017) 212, arXiv:1606.08197.

[9] R.L. Thews, M. Schroedter, J. Rafelski, Enhanced J/ψ production in deconfined quark matter, Phys. Rev. C 63 (2001) 054905, arXiv:hep-ph/0007323.

[10] P. Braun-Munzinger, J. Stachel, (Non)thermal aspects of charmonium production and a new look at J/ψ suppression, Phys. Lett. B 490 (2000) 196, arXiv:nucl-th/0007059.

[11] M. Hirai, S. Kumano, T.-H. Nagai, Determination of nuclear parton distribution functions and their uncertainties in next-to-leading order, Phys. Rev. C 76 (2007) 065207, arXiv:0709.3038.

[12] K.J. Eskola, H. Paukkunen, C.A. Salgado, EPS09: a new generation of NLO and LO nuclear parton distribution functions, J. High Energy Phys. 04 (2009) 065, arXiv:0902.4154.

[13] D. de Florian, R. Sassot, P. Zurita, M. Stratmann, Global analysis of nuclear parton distributions, Phys. Rev. D 85 (2012) 074028, arXiv:1112.6324.

[14] K. Kovarik, et al., nCTEQ15 – global analysis of nuclear parton distributions with uncertainties in the CTEQ framework, Phys. Rev. D 93 (2016) 085037, arXiv:1509.00792.

[15] K.J. Eskola, P. Paakkinen, H. Paukkunen, C.A. Salgado, EPPS16: nuclear parton distributions with LHC data, Eur. Phys. J. C 77 (2017) 163, arXiv:1612.05741.

[16] F. Gelis, E. Iancu, J. Jalilian-Marian, R. Venugopalan, The Color Glass Condensate, Annu. Rev. Nucl. Part. Sci. 60 (2010) 463, arXiv:1002.0333.

[17] H. Fujii, F. Gelis, R. Venugopalan, Quark pair production in high energy pA collisions: general features, Nucl. Phys. A 780 (2006) 146, arXiv:hep-ph/0603099.

[18] R. Vogt, Shadowing and absorption effects on J/ψ production in dA collisions, Phys. Rev. C 71 (2005) 054902, arXiv:hep-ph/0411378.

[19] E.G. Ferreiro, F. Fleuret, J.P. Lansberg, A. Rakotozafindrabe, Cold nuclear matter effects on J/ψ production: intrinsic and extrinsic transverse momentum effects, Phys. Lett. B 680 (2009) 50, arXiv:0809.4684.

[20] R. Vogt, Cold nuclear matter effects on J/ψ and Υ production at energies available at the CERN Large Hadron Collider (LHC), Phys. Rev. C 81 (2010) 044903, arXiv:1003.3497.

[21] J.-P. Lansberg, H.-S. Shao, Towards an automated tool to evaluate the impact of the nuclear modification of the gluon density on quarkonium, D and B meson production in proton-nucleus collisions, Eur. Phys. J. C 77 (2017) 1, arXiv:1610.05382.

[22] H. Fujii, K. Watanabe, Heavy quark pair production in high energy pA collisions: quarkonium, Nucl. Phys. A 915 (2013) 1, arXiv:1304.2221.

[23] Y.-Q. Ma, R. Venugopalan, H.-F. Zhang, J/ψ production and suppression in high energy proton-nucleus collisions, Phys. Rev. D 92 (2015) 071901, arXiv:1503.07772.

[24] B. Ducloué, T. Lappi, H. Mäntysaari, Forward J/ψ production in proton-nucleus collisions at high energy, Phys. Rev. D 91 (2015) 114005, arXiv:1503.02789.

[25] F. Arleo, S. Peigne, Heavy-quarkonium suppression in pA collisions from parton energy loss in cold QCD matter, J. High Energy Phys. 03 (2013) 122, arXiv:1212.0434.

[26] ALICE collaboration, B. Abelev, et al., J/ψ production and nuclear effects in pPb collisions at $\sqrt{s_{NN}} = 5.02$ TeV, J. High Energy Phys. 02 (2014) 073, arXiv:1308.6726.

[27] LHCb collaboration, R. Aaij, et al., Study of J/ψ production and cold nuclear matter effects in pPb collisions at $\sqrt{s_{NN}} = 5$ TeV, J. High Energy Phys. 02 (2014) 072, arXiv:1308.6729.

[28] ALICE collaboration, J. Adam, et al., Rapidity and transverse-momentum dependence of the inclusive J/ψ nuclear modification factor in pPb collisions at $\sqrt{s_{NN}} = 5.02$ TeV, J. High Energy Phys. 06 (2015) 055, arXiv:1503.07179.

[29] ALICE collaboration, J. Adam, et al., Centrality dependence of inclusive J/ψ production in pPb collisions at $\sqrt{s_{NN}} = 5.02$ TeV, J. High Energy Phys. 11 (2015) 127, arXiv:1506.08808.

[30] ATLAS collaboration, G. Aad, et al., Measurement of differential J/ψ production cross sections and forward-backward ratios in pPb collisions with the ATLAS detector, Phys. Rev. C 92 (2015) 034904, arXiv:1505.08141.

[31] CMS collaboration, A.M. Sirunyan, et al., Measurement of prompt and non-prompt J/ψ production in pp and pPb collisions at $\sqrt{s_{NN}} = 5.02$ TeV, Eur. Phys. J. C 77 (2017) 269, arXiv:1702.01462.

[32] ALICE collaboration, B.B. Abelev, et al., Suppression of $\psi(2S)$ production in pPb collisions at $\sqrt{s_{NN}} = 5.02$ TeV, J. High Energy Phys. 12 (2014) 073, arXiv:1405.3796.

[33] ALICE collaboration, J. Adam, et al., Centrality dependence of $\psi(2S)$ suppression in pPb collisions at $\sqrt{s_{NN}} = 5.02$ TeV, J. High Energy Phys. 06 (2016) 050, arXiv:1603.02816.

[34] LHCb collaboration, R. Aaij, et al., Study of $\psi(2S)$ production cross-sections and cold nuclear matter effects in pPb collisions at $\sqrt{s_{NN}} = 5$ TeV, J. High Energy Phys. 03 (2016) 133, arXiv:1601.07878.

[35] PHENIX collaboration, A. Adare, et al., Nuclear modification of ψ', χ_c, and J/ψ production in d+Au collisions at $\sqrt{s_{NN}} = 200$ GeV, Phys. Rev. Lett. 111 (2013) 202301, arXiv:1305.5516.

[36] PHENIX collaboration, A. Adare, et al., Measurement of the relative yields of $\psi(2S)$ to $\psi(1S)$ mesons produced at forward and backward rapidity in $p + p$, $p + Al$, $p + Au$, and $^3He + Au$ collisions at $\sqrt{s_{NN}} = 200$ GeV, Phys. Rev. C 95 (2017) 034904, arXiv:1609.06550.

[37] E.G. Ferreiro, Excited charmonium suppression in proton-nucleus collisions as a consequence of comovers, Phys. Lett. B 749 (2015) 98, arXiv:1411.0549.

[38] X. Du, R. Rapp, Sequential regeneration of charmonia in heavy-ion collisions, Nucl. Phys. A 943 (2015) 147, arXiv:1504.00670.

[39] LHCb collaboration, A.A. Alves Jr., et al., The LHCb detector at the LHC, J. Instrum. 3 (2008) S08005.

[40] LHCb collaboration, R. Aaij, et al., LHCb detector performance, Int. J. Mod. Phys. A 30 (2015) 1530022, arXiv:1412.6352.

[41] R. Aaij, et al., Performance of the LHCb Vertex Locator, J. Instrum. 9 (2014), P09007, arXiv:1405.7808.

[42] R. Arink, et al., Performance of the LHCb Outer Tracker, J. Instrum. 9 (2014), P01002, arXiv:1311.3893.

[43] M. Adinolfi, et al., Performance of the LHCb RICH detector at the LHC, Eur. Phys. J. C 73 (2013) 2431, arXiv:1211.6759.

[44] A.A. Alves Jr., et al., Performance of the LHCb muon system, J. Instrum. 8 (2013), P02022, arXiv:1211.1346.

[45] LHCb collaboration, R. Aaij, et al., Measurement of forward J/ψ production cross-sections in pp collisions at $\sqrt{s} = 13$ TeV, J. High Energy Phys. 10 (2015) 172, arXiv:1509.00771.

[46] Particle Data Group, C. Patrignani, et al., Review of particle physics, Chin. Phys. C 40 (2016) 100001.

[47] LHCb collaboration, R. Aaij, et al., Precision luminosity measurements at LHCb, J. Instrum. 9 (2014), P12005, arXiv:1410.0149.

[48] G. Dujany, B. Storaci, Real-time alignment and calibration of the LHCb detector in Run II, J. Phys. Conf. Ser. 664 (2015) 082010.

[49] R. Aaij, et al., The LHCb trigger and its performance in 2011, J. Instrum. 8 (2013), P04022, arXiv:1211.3055.

[50] R. Aaij, et al., Tesla: an application for real-time data analysis in high energy physics, Comput. Phys. Commun. 208 (2016) 35, arXiv:1604.05596.

[51] LHCb collaboration, R. Aaij, et al., Study of J/ψ production in jets, Phys. Rev. Lett. 118 (2017) 192001, arXiv:1701.05116.

[52] T. Skwarnicki, A Study of the Radiative Cascade Transitions Between the Upsilon-Prime and Upsilon Resonances, PhD thesis, Institute of Nuclear Physics, Krakow, 1986, DESY-F31-86-02.

[53] T. Pierog, et al., EPOS LHC: test of collective hadronization with data measured at the CERN Large Hadron Collider, Phys. Rev. C 92 (2015) 034906, arXiv:1306.0121.

[54] T. Sjöstrand, S. Mrenna, P. Skands, A brief introduction to PYTHIA 8.1, Comput. Phys. Commun. 178 (2008) 852, arXiv:0710.3820.

[55] D.J. Lange, The EvtGen particle decay simulation package, Nucl. Instrum. Methods A 462 (2001) 152.

[56] P. Golonka, Z. Was, PHOTOS Monte Carlo: a precision tool for QED corrections in Z and W decays, Eur. Phys. J. C 45 (2006) 97, arXiv:hep-ph/0506026.

[57] Geant4 collaboration, J. Allison, et al., Geant4 developments and applications, IEEE Trans. Nucl. Sci. 53 (2006) 270;
Geant4 collaboration, S. Agostinelli, et al., Geant4: A simulation toolkit, Nucl. Instrum. Methods A 506 (2003) 250.

[58] M. Clemencic, et al., The LHCb simulation application, Gauss: design, evolution and experience, J. Phys. Conf. Ser. 331 (2011) 032023.

[59] LHCb collaboration, R. Aaij, et al., Measurement of the track reconstruction efficiency at LHCb, J. Instrum. 10 (2015), P02007, arXiv:1408.1251.

[60] L. Anderlini, et al., The PIDCalib package, LHCb-PUB-2016-021.

[61] ALICE collaboration, B. Abelev, et al., J/ψ polarization in pp collisions at $\sqrt{s} = 7$ TeV, Phys. Rev. Lett. 108 (2012) 082001, arXiv:1111.1630.

[62] LHCb collaboration, R. Aaij, et al., Measurement of J/ψ polarization in pp collisions at $\sqrt{s} = 7$ TeV, Eur. Phys. J. C 73 (2013) 2631, arXiv:1307.6379.

[63] LHCb collaboration, R. Aaij, et al., Production of J/ψ and Υ mesons in pp collisions at $\sqrt{s} = 8$ TeV, J. High Energy Phys. 06 (2013) 064, arXiv:1304.6977.

[64] LHCb collaboration, R. Aaij, et al., Measurement of J/ψ production in pp collisions at $\sqrt{s} = 7$ TeV, Eur. Phys. J. C 71 (2011) 1645, arXiv:1103.0423.

[65] ALICE and LHCb collaborations, Reference pp cross-sections for J/ψ studies in proton-lead collisions at $\sqrt{s_{NN}} = 5.02$ TeV and comparisons between ALICE and LHCb results, LHCb-CONF-2013-013, ALICE-PUBLIC-2013-002.

[66] H.-S. Shao, HELAC-Onia: an automatic matrix element generator for heavy quarkonium physics, Comput. Phys. Commun. 184 (2013) 2562, arXiv:1212.5293.

[67] H.-S. Shao, HELAC-Onia 2.0: an upgraded matrix-element and event generator for heavy quarkonium physics, Comput. Phys. Commun. 198 (2016) 238, arXiv:1507.03435.

[68] B. Ducloué, T. Lappi, H. Mäntysaari, Forward J/ψ production at high energy: centrality dependence and mean transverse momentum, Phys. Rev. D 94 (2016) 074031, arXiv:1605.05680.

[69] M. Cacciari, M. Greco, P. Nason, The p_T spectrum in heavy-flavour hadroproduction, J. High Energy Phys. 05 (1998) 007, arXiv:hep-ph/9803400.

[70] M. Cacciari, S. Frixione, P. Nason, The p_T spectrum in heavy-flavour photoproduction, J. High Energy Phys. 03 (2001) 006, arXiv:hep-ph/0102134.

[71] CMS collaboration, S. Chatrchyan, et al., Observation of long-range near-side angular correlations in pPb collisions at the LHC, Phys. Lett. B 718 (2013) 795, arXiv:1210.5482.

[72] ALICE collaboration, B. Abelev, et al., Long-range angular correlations on the near and away side in pPb collisions at $\sqrt{s_{NN}} = 5.02$ TeV, Phys. Lett. B 719 (2013) 29, arXiv:1212.2001.

[73] ATLAS collaboration, G. Aad, et al., Observation of associated near-side and away-side long-range correlations in $\sqrt{s_{NN}} = 5.02$ TeV proton-lead collisions with the ATLAS detector, Phys. Rev. Lett. 110 (2013) 182302, arXiv:1212.5198.

[74] PHENIX collaboration, A. Adare, et al., Quadrupole anisotropy in dihadron azimuthal correlations in central $d + Au$ collisions at $\sqrt{s_{NN}} = 200$ GeV, Phys. Rev. Lett. 111 (2013) 212301, arXiv:1303.1794.

[75] A. Beraudo, et al., Heavy-flavour production in high-energy d-Au and p-Pb collisions, J. High Energy Phys. 03 (2016) 123, arXiv:1512.05186.

LHCb Collaboration

R. Aaij [40], B. Adeva [39], M. Adinolfi [48], Z. Ajaltouni [5], S. Akar [59], J. Albrecht [10], F. Alessio [40], M. Alexander [53], A. Alfonso Albero [38], S. Ali [43], G. Alkhazov [31], P. Alvarez Cartelle [55], A.A. Alves Jr [59], S. Amato [2],

S. Amerio [23], Y. Amhis [7], L. An [3], L. Anderlini [18], G. Andreassi [41], M. Andreotti [17,g], J.E. Andrews [60],
R.B. Appleby [56], F. Archilli [43], P. d'Argent [12], J. Arnau Romeu [6], A. Artamonov [37], M. Artuso [61],
E. Aslanides [6], G. Auriemma [26], M. Baalouch [5], I. Babuschkin [56], S. Bachmann [12], J.J. Back [50], A. Badalov [38],
C. Baesso [62], S. Baker [55], V. Balagura [7,c], W. Baldini [17], A. Baranov [35], R.J. Barlow [56], C. Barschel [40],
S. Barsuk [7], W. Barter [56], F. Baryshnikov [32], M. Baszczyk [27,l], V. Batozskaya [29], V. Battista [41], A. Bay [41],
L. Beaucourt [4], J. Beddow [53], F. Bedeschi [24], I. Bediaga [1], A. Beiter [61], L.J. Bel [43], N. Beliy [63], V. Bellee [41],
N. Belloli [21,i], K. Belous [37], I. Belyaev [32], E. Ben-Haim [8], G. Bencivenni [19], S. Benson [43], S. Beranek [9],
A. Berezhnoy [33], R. Bernet [42], D. Berninghoff [12], E. Bertholet [8], A. Bertolin [23], C. Betancourt [42], F. Betti [15],
M.-O. Bettler [40], M. van Beuzekom [43], Ia. Bezshyiko [42], S. Bifani [47], P. Billoir [8], A. Birnkraut [10],
A. Bitadze [56], A. Bizzeti [18,u], M.B. Bjoern [57], T. Blake [50], F. Blanc [41], J. Blouw [11,†], S. Blusk [61], V. Bocci [26],
T. Boettcher [58], A. Bondar [36,w], N. Bondar [31], W. Bonivento [16], I. Bordyuzhin [32], A. Borgheresi [21,i],
S. Borghi [56], M. Borisyak [35], M. Borsato [39], M. Borysova [46], F. Bossu [7], M. Boubdir [9], T.J.V. Bowcock [54],
E. Bowen [42], C. Bozzi [17,40], S. Braun [12], T. Britton [61], J. Brodzicka [56], D. Brundu [16], E. Buchanan [48],
C. Burr [56], A. Bursche [16,f], J. Buytaert [40], W. Byczynski [40], S. Cadeddu [16], H. Cai [64], R. Calabrese [17,g],
R. Calladine [47], M. Calvi [21,i], M. Calvo Gomez [38,m], A. Camboni [38], P. Campana [19], D.H. Campora Perez [40],
L. Capriotti [56], A. Carbone [15,e], G. Carboni [25,j], R. Cardinale [20,h], A. Cardini [16], P. Carniti [21,i], L. Carson [52],
K. Carvalho Akiba [2], G. Casse [54], L. Cassina [21,i], L. Castillo Garcia [41], M. Cattaneo [40], G. Cavallero [20,40,h],
R. Cenci [24,t], D. Chamont [7], M. Charles [8], Ph. Charpentier [40], G. Chatzikonstantinidis [47], M. Chefdeville [4],
S. Chen [56], S.F. Cheung [57], S.-G. Chitic [40], V. Chobanova [39], M. Chrzaszcz [42,27], A. Chubykin [31],
X. Cid Vidal [39], G. Ciezarek [43], P.E.L. Clarke [52], M. Clemencic [40], H.V. Cliff [49], J. Closier [40], V. Coco [59],
J. Cogan [6], E. Cogneras [5], V. Cogoni [16,f], L. Cojocariu [30], P. Collins [40], T. Colombo [40],
A. Comerma-Montells [12], A. Contu [40], A. Cook [48], G. Coombs [40], S. Coquereau [38], G. Corti [40], M. Corvo [17,g],
C.M. Costa Sobral [50], B. Couturier [40], G.A. Cowan [52], D.C. Craik [52], A. Crocombe [50], M. Cruz Torres [62],
R. Currie [52], C. D'Ambrosio [40], F. Da Cunha Marinho [2], E. Dall'Occo [43], J. Dalseno [48], A. Davis [3],
O. De Aguiar Francisco [54], K. De Bruyn [6], S. De Capua [56], M. De Cian [12], J.M. De Miranda [1], L. De Paula [2],
M. De Serio [14,d], P. De Simone [19], C.T. Dean [53], D. Decamp [4], L. Del Buono [8], H.-P. Dembinski [11],
M. Demmer [10], A. Dendek [28], D. Derkach [35], O. Deschamps [5], F. Dettori [54], B. Dey [65], A. Di Canto [40],
P. Di Nezza [19], H. Dijkstra [40], F. Dordei [40], M. Dorigo [41], A. Dosil Suárez [39], L. Douglas [53], A. Dovbnya [45],
K. Dreimanis [54], L. Dufour [43], G. Dujany [8], K. Dungs [40], P. Durante [40], R. Dzhelyadin [37], M. Dziewiecki [12],
A. Dziurda [40], A. Dzyuba [31], N. Déléage [4], S. Easo [51], M. Ebert [52], U. Egede [55], V. Egorychev [32],
S. Eidelman [36,w], S. Eisenhardt [52], U. Eitschberger [10], R. Ekelhof [10], L. Eklund [53], S. Ely [61], S. Esen [12],
H.M. Evans [49], T. Evans [57], A. Falabella [15], N. Farley [47], S. Farry [54], R. Fay [54], D. Fazzini [21,i], L. Federici [25],
D. Ferguson [52], G. Fernandez [38], P. Fernandez Declara [40], A. Fernandez Prieto [39], F. Ferrari [15],
F. Ferreira Rodrigues [2], M. Ferro-Luzzi [40], S. Filippov [34], R.A. Fini [14], M. Fiore [17,g], M. Fiorini [17,g],
M. Firlej [28], C. Fitzpatrick [41], T. Fiutowski [28], F. Fleuret [7,b], K. Fohl [40], M. Fontana [16,40], F. Fontanelli [20,h],
D.C. Forshaw [61], R. Forty [40], V. Franco Lima [54], M. Frank [40], C. Frei [40], J. Fu [22,q], W. Funk [40], E. Furfaro [25,j],
C. Färber [40], E. Gabriel [52], A. Gallas Torreira [39], D. Galli [15,e], S. Gallorini [23], S. Gambetta [52],
M. Gandelman [2], P. Gandini [57], Y. Gao [3], L.M. Garcia Martin [70], J. García Pardiñas [39], J. Garra Tico [49],
L. Garrido [38], P.J. Garsed [49], D. Gascon [38], C. Gaspar [40], L. Gavardi [10], G. Gazzoni [5], D. Gerick [12],
E. Gersabeck [12], M. Gersabeck [56], T. Gershon [50], Ph. Ghez [4], S. Gianì [41], V. Gibson [49], O.G. Girard [41],
L. Giubega [30], K. Gizdov [52], V.V. Gligorov [8], D. Golubkov [32], A. Golutvin [55,40], A. Gomes [1,a], I.V. Gorelov [33],
C. Gotti [21,i], E. Govorkova [43], J.P. Grabowski [12], R. Graciani Diaz [38], L.A. Granado Cardoso [40], E. Graugés [38],
E. Graverini [42], G. Graziani [18], A. Grecu [30], R. Greim [9], P. Griffith [16], L. Grillo [21,40,i], L. Gruber [40],
B.R. Gruberg Cazon [57], O. Grünberg [67], E. Gushchin [34], Yu. Guz [37], T. Gys [40], C. Göbel [62], T. Hadavizadeh [57],
C. Hadjivasiliou [5], G. Haefeli [41], C. Haen [40], S.C. Haines [49], B. Hamilton [60], X. Han [12], T. Hancock [57],
S. Hansmann-Menzemer [12], N. Harnew [57], S.T. Harnew [48], J. Harrison [56], C. Hasse [40], M. Hatch [40], J. He [63],
M. Hecker [55], K. Heinicke [10], A. Heister [9], K. Hennessy [54], P. Henrard [5], L. Henry [70], E. van Herwijnen [40],
M. Heß [67], A. Hicheur [2], D. Hill [57], C. Hombach [56], P.H. Hopchev [41], Z.-C. Huard [59], W. Hulsbergen [43],
T. Humair [55], M. Hushchyn [35], D. Hutchcroft [54], P. Ibis [10], M. Idzik [28], P. Ilten [58], R. Jacobsson [40],
J. Jalocha [57], E. Jans [43], A. Jawahery [60], F. Jiang [3], M. John [57], D. Johnson [40], C.R. Jones [49], C. Joram [40],
B. Jost [40], N. Jurik [57], S. Kandybei [45], M. Karacson [40], J.M. Kariuki [48], S. Karodia [53], M. Kecke [12],
M. Kelsey [61], M. Kenzie [49], T. Ketel [44], E. Khairullin [35], B. Khanji [12], C. Khurewathanakul [41], T. Kirn [9],

S. Klaver [56], K. Klimaszewski [29], T. Klimkovich [11], S. Koliiev [46], M. Kolpin [12], I. Komarov [41], R. Kopecna [12],
P. Koppenburg [43], A. Kosmyntseva [32], S. Kotriakhova [31], M. Kozeiha [5], L. Kravchuk [34], M. Kreps [50],
P. Krokovny [36,w], F. Kruse [10], W. Krzemien [29], W. Kucewicz [27,l], M. Kucharczyk [27], V. Kudryavtsev [36,w],
A.K. Kuonen [41], K. Kurek [29], T. Kvaratskheliya [32,40], D. Lacarrere [40], G. Lafferty [56], A. Lai [16], G. Lanfranchi [19],
C. Langenbruch [9], T. Latham [50], C. Lazzeroni [47], R. Le Gac [6], J. van Leerdam [43], A. Leflat [33,40], J. Lefrançois [7],
R. Lefèvre [5], F. Lemaitre [40], E. Lemos Cid [39], O. Leroy [6], T. Lesiak [27], B. Leverington [12], T. Li [3], Y. Li [7], Z. Li [61],
T. Likhomanenko [35,68], R. Lindner [40], F. Lionetto [42], X. Liu [3], D. Loh [50], I. Longstaff [53], J.H. Lopes [2],
D. Lucchesi [23,o], M. Lucio Martinez [39], H. Luo [52], A. Lupato [23], E. Luppi [17,g], O. Lupton [40], A. Lusiani [24],
X. Lyu [63], F. Machefert [7], F. Maciuc [30], V. Macko [41], P. Mackowiak [10], B. Maddock [59],
S. Maddrell-Mander [48], O. Maev [31], K. Maguire [56], D. Maisuzenko [31], M.W. Majewski [28], S. Malde [57],
A. Malinin [68], T. Maltsev [36], G. Manca [16,f], G. Mancinelli [6], P. Manning [61], D. Marangotto [22,q], J. Maratas [5,v],
J.F. Marchand [4], U. Marconi [15], C. Marin Benito [38], M. Marinangeli [41], P. Marino [24,t], J. Marks [12],
G. Martellotti [26], M. Martin [6], M. Martinelli [41], D. Martinez Santos [39], F. Martinez Vidal [70],
D. Martins Tostes [2], L.M. Massacrier [7], A. Massafferri [1], R. Matev [40], A. Mathad [50], Z. Mathe [40],
C. Matteuzzi [21], A. Mauri [42], E. Maurice [7,b], B. Maurin [41], A. Mazurov [47], M. McCann [55,40], A. McNab [56],
R. McNulty [13], J.V. Mead [54], B. Meadows [59], C. Meaux [6], F. Meier [10], N. Meinert [67], D. Melnychuk [29],
M. Merk [43], A. Merli [22,40,q], E. Michielin [23], D.A. Milanes [66], E. Millard [50], M.-N. Minard [4], L. Minzoni [17],
D.S. Mitzel [12], A. Mogini [8], J. Molina Rodriguez [1], T. Mombacher [10], I.A. Monroy [66], S. Monteil [5],
M. Morandin [23], M.J. Morello [24,t], O. Morgunova [68], J. Moron [28], A.B. Morris [52], R. Mountain [61],
F. Muheim [52], M. Mulder [43], M. Mussini [15], D. Müller [56], J. Müller [10], K. Müller [42], V. Müller [10], P. Naik [48],
T. Nakada [41], R. Nandakumar [51], A. Nandi [57], I. Nasteva [2], M. Needham [52], N. Neri [22,40], S. Neubert [12],
N. Neufeld [40], M. Neuner [12], T.D. Nguyen [41], C. Nguyen-Mau [41,n], S. Nieswand [9], R. Niet [10], N. Nikitin [33],
T. Nikodem [12], A. Nogay [68], D.P. O'Hanlon [50], A. Oblakowska-Mucha [28], V. Obraztsov [37], S. Ogilvy [19],
R. Oldeman [16,f], C.J.G. Onderwater [71], A. Ossowska [27], J.M. Otalora Goicochea [2], P. Owen [42],
A. Oyanguren [70], P.R. Pais [41], A. Palano [14,d], M. Palutan [19,40], A. Papanestis [51], M. Pappagallo [14,d],
L.L. Pappalardo [17,g], C. Pappenheimer [59], W. Parker [60], C. Parkes [56], G. Passaleva [18], A. Pastore [14,d],
M. Patel [55], C. Patrignani [15,e], A. Pearce [40], A. Pellegrino [43], G. Penso [26], M. Pepe Altarelli [40], S. Perazzini [40],
P. Perret [5], L. Pescatore [41], K. Petridis [48], A. Petrolini [20,h], A. Petrov [68], M. Petruzzo [22,q],
E. Picatoste Olloqui [38], B. Pietrzyk [4], M. Pikies [27], D. Pinci [26], A. Pistone [20,h], A. Piucci [12], V. Placinta [30],
S. Playfer [52], M. Plo Casasus [39], T. Poikela [40], F. Polci [8], M. Poli Lener [19], A. Poluektov [50,36], I. Polyakov [61],
E. Polycarpo [2], G.J. Pomery [48], S. Ponce [40], A. Popov [37], D. Popov [11,40], S. Poslavskii [37], C. Potterat [2],
E. Price [48], J. Prisciandaro [39], C. Prouve [48], V. Pugatch [46], A. Puig Navarro [42], H. Pullen [57], G. Punzi [24,p],
W. Qian [50], R. Quagliani [7,48], B. Quintana [5], B. Rachwal [28], J.H. Rademacker [48], M. Rama [24],
M. Ramos Pernas [39], M.S. Rangel [2], I. Raniuk [45,†], F. Ratnikov [35], G. Raven [44], M. Ravonel Salzgeber [40],
M. Reboud [4], F. Redi [55], S. Reichert [10], A.C. dos Reis [1], C. Remon Alepuz [70], V. Renaudin [7], S. Ricciardi [51],
S. Richards [48], M. Rihl [40], K. Rinnert [54], V. Rives Molina [38], P. Robbe [7], A.B. Rodrigues [1], E. Rodrigues [59],
J.A. Rodriguez Lopez [66], P. Rodriguez Perez [56,†], A. Rogozhnikov [35], S. Roiser [40], A. Rollings [57],
V. Romanovskiy [37], A. Romero Vidal [39], J.W. Ronayne [13], M. Rotondo [19], M.S. Rudolph [61], T. Ruf [40],
P. Ruiz Valls [70], J. Ruiz Vidal [70], J.J. Saborido Silva [39], E. Sadykhov [32], N. Sagidova [31], B. Saitta [16,f],
V. Salustino Guimaraes [1], D. Sanchez Gonzalo [38], C. Sanchez Mayordomo [70], B. Sanmartin Sedes [39],
R. Santacesaria [26], C. Santamarina Rios [39], M. Santimaria [19], E. Santovetti [25,j], G. Sarpis [56], A. Sarti [26],
C. Satriano [26,s], A. Satta [25], D.M. Saunders [48], D. Savrina [32,33], S. Schael [9], M. Schellenberg [10],
M. Schiller [53], H. Schindler [40], M. Schlupp [10], M. Schmelling [11], T. Schmelzer [10], B. Schmidt [40],
O. Schneider [41], A. Schopper [40], H.F. Schreiner [59], K. Schubert [10], M. Schubiger [41], M.-H. Schune [7],
R. Schwemmer [40], B. Sciascia [19], A. Sciubba [26,k], A. Semennikov [32], A. Sergi [47], N. Serra [42], J. Serrano [6],
L. Sestini [23], P. Seyfert [40], M. Shapkin [37], I. Shapoval [45], Y. Shcheglov [31], T. Shears [54], L. Shekhtman [36,w],
V. Shevchenko [68], B.G. Siddi [17,40], R. Silva Coutinho [42], L. Silva de Oliveira [2], G. Simi [23,o], S. Simone [14,d],
M. Sirendi [49], N. Skidmore [48], T. Skwarnicki [61], E. Smith [55], I.T. Smith [52], J. Smith [49], M. Smith [55],
l. Soares Lavra [1], M.D. Sokoloff [59], F.J.P. Soler [53], B. Souza De Paula [2], B. Spaan [10], P. Spradlin [53],
S. Sridharan [40], F. Stagni [40], M. Stahl [12], S. Stahl [40], P. Stefko [41], S. Stefkova [55], O. Steinkamp [42],
S. Stemmle [12], O. Stenyakin [37], H. Stevens [10], S. Stone [61], B. Storaci [42], S. Stracka [24,p], M.E. Stramaglia [41],
M. Straticiuc [30], U. Straumann [42], L. Sun [64], W. Sutcliffe [55], K. Swientek [28], V. Syropoulos [44],

M. Szczekowski [29], T. Szumlak [28], M. Szymanski [63], S. T'Jampens [4], A. Tayduganov [6], T. Tekampe [10], G. Tellarini [17,g], F. Teubert [40], E. Thomas [40], J. van Tilburg [43], M.J. Tilley [55], V. Tisserand [4], M. Tobin [41], S. Tolk [49], L. Tomassetti [17,g], D. Tonelli [24], S. Topp-Joergensen [57], F. Toriello [61], R. Tourinho Jadallah Aoude [1], E. Tournefier [4], M. Traill [53], M.T. Tran [41], M. Tresch [42], A. Trisovic [40], A. Tsaregorodtsev [6], P. Tsopelas [43], A. Tully [49], N. Tuning [43], A. Ukleja [29], A. Ustyuzhanin [35], U. Uwer [12], C. Vacca [16,f], A. Vagner [69], V. Vagnoni [15,40], A. Valassi [40], S. Valat [40], G. Valenti [15], R. Vazquez Gomez [19], P. Vazquez Regueiro [39], S. Vecchi [17], M. van Veghel [43], J.J. Velthuis [48], M. Veltri [18,r], G. Veneziano [57], A. Venkateswaran [61], T.A. Verlage [9], M. Vernet [5], M. Vesterinen [57], J.V. Viana Barbosa [40], B. Viaud [7], D. Vieira [63], M. Vieites Diaz [39], H. Viemann [67], X. Vilasis-Cardona [38,m], M. Vitti [49], V. Volkov [33], A. Vollhardt [42], B. Voneki [40], A. Vorobyev [31], V. Vorobyev [36,w], C. Voß [9], J.A. de Vries [43], C. Vázquez Sierra [39], R. Waldi [67], C. Wallace [50], R. Wallace [13], J. Walsh [24], J. Wang [61], D.R. Ward [49], H.M. Wark [54], N.K. Watson [47], D. Websdale [55], A. Weiden [42], M. Whitehead [40], J. Wicht [50], G. Wilkinson [57,40], M. Wilkinson [61], M. Williams [56], M.P. Williams [47], M. Williams [58], T. Williams [47], F.F. Wilson [51], J. Wimberley [60], M.A. Winn [7,*], J. Wishahi [10], W. Wislicki [29], M. Witek [27], G. Wormser [7], S.A. Wotton [49], K. Wraight [53], K. Wyllie [40], Y. Xie [65], Z. Xu [4], Z. Yang [3], Z. Yang [60], Y. Yao [61], H. Yin [65], J. Yu [65], X. Yuan [61], O. Yushchenko [37], K.A. Zarebski [47], M. Zavertyaev [11,c], L. Zhang [3], Y. Zhang [7], A. Zhelezov [12], Y. Zheng [63], X. Zhu [3], V. Zhukov [33], J.B. Zonneveld [52], S. Zucchelli [15]

[1] *Centro Brasileiro de Pesquisas Físicas (CBPF), Rio de Janeiro, Brazil*
[2] *Universidade Federal do Rio de Janeiro (UFRJ), Rio de Janeiro, Brazil*
[3] *Center for High Energy Physics, Tsinghua University, Beijing, China*
[4] *LAPP, Université Savoie Mont-Blanc, CNRS/IN2P3, Annecy-Le-Vieux, France*
[5] *Clermont Université, Université Blaise Pascal, CNRS/IN2P3, LPC, Clermont-Ferrand, France*
[6] *CPPM, Aix-Marseille Université, CNRS/IN2P3, Marseille, France*
[7] *LAL, Université Paris-Sud, CNRS/IN2P3, Orsay, France*
[8] *LPNHE, Université Pierre et Marie Curie, Université Paris Diderot, CNRS/IN2P3, Paris, France*
[9] *I. Physikalisches Institut, RWTH Aachen University, Aachen, Germany*
[10] *Fakultät Physik, Technische Universität Dortmund, Dortmund, Germany*
[11] *Max-Planck-Institut für Kernphysik (MPIK), Heidelberg, Germany*
[12] *Physikalisches Institut, Ruprecht-Karls-Universität Heidelberg, Heidelberg, Germany*
[13] *School of Physics, University College Dublin, Dublin, Ireland*
[14] *Sezione INFN di Bari, Bari, Italy*
[15] *Sezione INFN di Bologna, Bologna, Italy*
[16] *Sezione INFN di Cagliari, Cagliari, Italy*
[17] *Universita e INFN, Ferrara, Ferrara, Italy*
[18] *Sezione INFN di Firenze, Firenze, Italy*
[19] *Laboratori Nazionali dell'INFN di Frascati, Frascati, Italy*
[20] *Sezione INFN di Genova, Genova, Italy*
[21] *Universita & INFN, Milano-Bicocca, Milano, Italy*
[22] *Sezione di Milano, Milano, Italy*
[23] *Sezione INFN di Padova, Padova, Italy*
[24] *Sezione INFN di Pisa, Pisa, Italy*
[25] *Sezione INFN di Roma Tor Vergata, Roma, Italy*
[26] *Sezione INFN di Roma La Sapienza, Roma, Italy*
[27] *Henryk Niewodniczanski Institute of Nuclear Physics Polish Academy of Sciences, Kraków, Poland*
[28] *AGH – University of Science and Technology, Faculty of Physics and Applied Computer Science, Kraków, Poland*
[29] *National Center for Nuclear Research (NCBJ), Warsaw, Poland*
[30] *Horia Hulubei National Institute of Physics and Nuclear Engineering, Bucharest-Magurele, Romania*
[31] *Petersburg Nuclear Physics Institute (PNPI), Gatchina, Russia*
[32] *Institute of Theoretical and Experimental Physics (ITEP), Moscow, Russia*
[33] *Institute of Nuclear Physics, Moscow State University (SINP MSU), Moscow, Russia*
[34] *Institute for Nuclear Research of the Russian Academy of Sciences (INR RAN), Moscow, Russia*
[35] *Yandex School of Data Analysis, Moscow, Russia*
[36] *Budker Institute of Nuclear Physics (SB RAS), Novosibirsk, Russia*
[37] *Institute for High Energy Physics (IHEP), Protvino, Russia*
[38] *ICCUB, Universitat de Barcelona, Barcelona, Spain*
[39] *Universidad de Santiago de Compostela, Santiago de Compostela, Spain*
[40] *European Organization for Nuclear Research (CERN), Geneva, Switzerland*
[41] *Institute of Physics, Ecole Polytechnique Fédérale de Lausanne (EPFL), Lausanne, Switzerland*
[42] *Physik-Institut, Universität Zürich, Zürich, Switzerland*
[43] *Nikhef National Institute for Subatomic Physics, Amsterdam, The Netherlands*
[44] *Nikhef National Institute for Subatomic Physics and VU University Amsterdam, Amsterdam, The Netherlands*
[45] *NSC Kharkiv Institute of Physics and Technology (NSC KIPT), Kharkiv, Ukraine*
[46] *Institute for Nuclear Research of the National Academy of Sciences (KINR), Kyiv, Ukraine*
[47] *University of Birmingham, Birmingham, United Kingdom*
[48] *H.H. Wills Physics Laboratory, University of Bristol, Bristol, United Kingdom*
[49] *Cavendish Laboratory, University of Cambridge, Cambridge, United Kingdom*
[50] *Department of Physics, University of Warwick, Coventry, United Kingdom*
[51] *STFC Rutherford Appleton Laboratory, Didcot, United Kingdom*
[52] *School of Physics and Astronomy, University of Edinburgh, Edinburgh, United Kingdom*
[53] *School of Physics and Astronomy, University of Glasgow, Glasgow, United Kingdom*

[54] *Oliver Lodge Laboratory, University of Liverpool, Liverpool, United Kingdom*
[55] *Imperial College London, London, United Kingdom*
[56] *School of Physics and Astronomy, University of Manchester, Manchester, United Kingdom*
[57] *Department of Physics, University of Oxford, Oxford, United Kingdom*
[58] *Massachusetts Institute of Technology, Cambridge, MA, United States*
[59] *University of Cincinnati, Cincinnati, OH, United States*
[60] *University of Maryland, College Park, MD, United States*
[61] *Syracuse University, Syracuse, NY, United States*
[62] *Pontifícia Universidade Católica do Rio de Janeiro (PUC-Rio), Rio de Janeiro, Brazil* [x]
[63] *University of Chinese Academy of Sciences, Beijing, China* [y]
[64] *School of Physics and Technology, Wuhan University, Wuhan, China* [y]
[65] *Institute of Particle Physics, Central China Normal University, Wuhan, Hubei, China* [y]
[66] *Departamento de Fisica, Universidad Nacional de Colombia, Bogota, Colombia* [z]
[67] *Institut für Physik, Universität Rostock, Rostock, Germany* [aa]
[68] *National Research Centre Kurchatov Institute, Moscow, Russia* [ab]
[69] *National Research Tomsk Polytechnic University, Tomsk, Russia* [ab]
[70] *Instituto de Fisica Corpuscular, Centro Mixto Universidad de Valencia – CSIC, Valencia, Spain* [ac]
[71] *Van Swinderen Institute, University of Groningen, Groningen, The Netherlands* [ad]

[*] Corresponding author.
   E-mail address: Michael.Winn@cern.ch (M.A. Winn).
[a] Universidade Federal do Triângulo Mineiro (UFTM), Uberaba-MG, Brazil.
[b] Laboratoire Leprince-Ringuet, Palaiseau, France.
[c] P.N. Lebedev Physical Institute, Russian Academy of Science (LPI RAS), Moscow, Russia.
[d] Università di Bari, Bari, Italy.
[e] Università di Bologna, Bologna, Italy.
[f] Università di Cagliari, Cagliari, Italy.
[g] Università di Ferrara, Ferrara, Italy.
[h] Università di Genova, Genova, Italy.
[i] Università di Milano Bicocca, Milano, Italy.
[j] Università di Roma Tor Vergata, Roma, Italy.
[k] Università di Roma La Sapienza, Roma, Italy.
[l] AGH - University of Science and Technology, Faculty of Computer Science, Electronics and Telecommunications, Kraków, Poland.
[m] LIFAELS, La Salle, Universitat Ramon Llull, Barcelona, Spain.
[n] Hanoi University of Science, Hanoi, Viet Nam.
[o] Università di Padova, Padova, Italy.
[p] Università di Pisa, Pisa, Italy.
[q] Università degli Studi di Milano, Milano, Italy.
[r] Università di Urbino, Urbino, Italy.
[s] Università della Basilicata, Potenza, Italy.
[t] Scuola Normale Superiore, Pisa, Italy.
[u] Università di Modena e Reggio Emilia, Modena, Italy.
[v] Iligan Institute of Technology (IIT), Iligan, Philippines.
[w] Novosibirsk State University, Novosibirsk, Russia.
[x] Associated to Universidade Federal do Rio de Janeiro (UFRJ), Rio de Janeiro, Brazil.
[y] Associated to Center for High Energy Physics, Tsinghua University, Beijing, China.
[z] Associated to LPNHE, Université Pierre et Marie Curie, Université Paris Diderot, CNRS/IN2P3, Paris, France.
[aa] Associated to Physikalisches Institut, Ruprecht-Karls-Universität Heidelberg, Heidelberg, Germany.
[ab] Associated to Institute of Theoretical and Experimental Physics (ITEP), Moscow, Russia.
[ac] Associated to ICCUB, Universitat de Barcelona, Barcelona, Spain.
[ad] Associated to Nikhef National Institute for Subatomic Physics, Amsterdam, The Netherlands.
[†] Deceased.